Suppressing the spin relaxation of electrons in silicon

Oleg Chalaev,[1] Yang Song,[1] and Hanan Dery[1,2,*]

[1]*Department of Electrical and Computer Engineering, University of Rochester, Rochester, New York 14627, USA*
[2]*Department of Physics and Astronomy, University of Rochester, Rochester, New York 14627, USA*

Uniaxial compressive strain along the [001] direction strongly suppresses the spin relaxation in silicon. When the strain level is large enough so that electrons are redistributed only in the two valleys along the strain axis, the dominant scattering mechanisms are quenched and electrons mainly experience intra-axis scattering processes (intravalley or intervalley scattering within valleys on the same crystal axis). We first derive the spin-flip matrix elements due to intra-axis electron scattering off impurities, and then provide a comprehensive model of the spin relaxation time due to all possible interactions of conduction-band electrons with impurities and phonons. We predict a nearly three orders of magnitude improvement in the spin relaxation time of $\sim 10^{19}$ cm^{-3} antimony-doped silicon (Si:Sb) at low temperatures.

I. INTRODUCTION

Silicon is a promising material choice for spintronic devices that require long spin lifetimes [1–10]. When electrons reach their saturation drift velocity, spin information in silicon can be transported over hundreds of microns [11–14], being compatible with on-chip interconnect length scales [15,16]. Transport over such distances is possible not only due to the relatively weak spin-orbit coupling of silicon atoms, but also to two major manifestations of the crystal space inversion symmetry. The first one is the spin degeneracy of the energy bands in centrosymmetric materials resulting in cancellation of the Dyakonov-Perel spin relaxation mechanism [17]. The second manifestation, first studied by Yafet, is that space inversion and time-reversal symmetries weaken the electron's spin-flip scattering amplitude due to interaction with phonons when $|\mathbf{k}_i \pm \mathbf{k}_f| a \ll 1$ [18–21]. Here, $\mathbf{k}_{i\,(f)}$ is the initial (final) electron's wave vector, and a is the lattice constant. In one case, the electron remains in the same valley, $|\mathbf{k}_i - \mathbf{k}_f| a \ll 1$, and in the other it is scattered to the opposite valley, $|\mathbf{k}_i + \mathbf{k}_f| a \ll 1$. The former denotes intravalley scattering, and the latter denotes intervalley scattering between opposite valleys, termed the g-process in silicon [22–25]. The relatively weak spin-flip scattering processes in silicon due to the intervalley g-process and the intravalley one can be generally classified as "intra-axis" scattering. These processes and other pertinent characteristics of the multivalley conduction band in silicon are shown in Fig. 1.

Contrary to the weak intra-axis spin-flip process in centrosymmetric materials, "interaxis" valley scattering can have a much larger spin-flip amplitude [18,26]. In this type of intervalley scattering, shown by the dashed-line arrow in Fig. 1(b) and termed the f-process in silicon [22,24,25], the initial and final valleys are not connected by time-reversal or space inversion symmetries. The electron transition between the valleys is mediated by interaction with shortwave phonons or short-range scattering off impurities [18,26]. While the contribution from shortwave phonons becomes negligible at low temperatures due to their large energy compared with

the thermal energy ($k_B T$), spin relaxation due to impurities is unavoidable at all temperatures. In either case, interaxis valley scattering is the dominant means to relax the spins of itinerant electrons in unstrained silicon or germanium [13,18,19,26–34].

Suppression of the detrimental interaxis valley scattering can be achieved by applying uniaxial compressive strain along the [001]-crystallographic direction in silicon, as shown in Fig. 1(c) [15,27,35–37]. This strain configuration lowers the energy edge for the pair of valleys along the strain axis, while the energy edge of the other four valleys is raised. For the valley splitting energy to be sufficiently large compared with $k_B T$, the strain levels should be of the order of 0.1% at 30 K and 1% at room temperature. Under these conditions, electrons populate the low-energy valley pair, and therefore they can only experience intra-axis scattering processes (intravalley and g-process). To date, there are no theoretical models that quantify the spin relaxation due to intra-axis electron scattering off impurities. The aim of this paper is to provide this missing component, and to compare the relative contributions of electron-phonon and electron-impurity interactions to spin relaxation.

Additional motivation for our work stems from the need to improve the electrical spin injection from ferromagnetic metals to heavily doped n-type silicon [38–68]. Because of the so-called conductivity and spin lifetime mismatch problem [69–72], electrical spin injection to semiconductors is largely limited to tunneling or ballistic injection of hot electrons [73–86]. In the former, electrons tunnel across the built-in potential barrier in the semiconductor side of the junction. The barrier is formed by the depletion region, existing both in direct metal-semiconductor Schottky contacts and metal-oxide-semiconductor structures with ultrathin oxide layers. Effective tunneling requires interface doping with donor concentrations of 10^{19} cm^{-3} or higher so that the thickness of the depletion region is only a few nanometers [73–76]. Such degenerate doping levels come with a penalty of enhanced spin relaxation due to electron-impurity scattering [87–98]. As we will show, application of strain to suppress the dominant interaxis valley scattering greatly increases the spin lifetime due to a much weaker effect of intra-axis scattering off impurities.
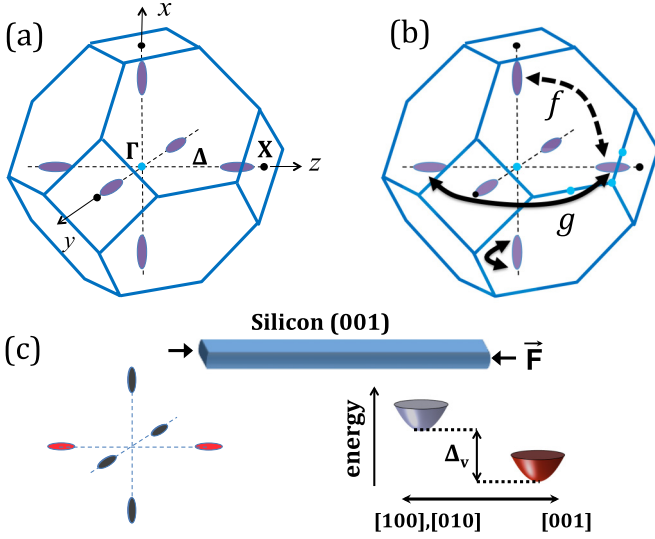
---

*hanan.dery@rochester.edu

FIG. 1. The conduction band in silicon includes six low-energy valleys located close to the X point along the Δ axis. (b) Examples of scattering processes in unstrained bulk silicon. Intra-axis processes, shown by solid-line arrows, include intravalley electron transitions as well as intervalley ones between time-reversal valleys, termed the g-process. The interaxis processes, shown by the dashed-line arrow, involve transitions between valleys that reside on different crystal axes (termed the f-process). (c) When applying compressive strain along one of the crystal axes, the two valleys along this axis are lowered in energy while the other four are raised. The dominant contribution to spin relaxation from interaxis processes is suppressed when the Fermi level lies well below the edge of the raised valleys (i.e., when $\Delta_v - E_F \gg k_B T$, where Δ_v is the strain-induced valley splitting).

Finally, it is emphasized that our focus in this work is on the spin relaxation of electrons in bulk silicon. As such, we do not consider quantization and interfacial effects, which may lead to additional spin dephasing mechanisms [1,8,37,99,100]. Similarly, we do not consider the strong effect that the strain has on the spin relaxation of holes [101–104]. Specifically, when the strain lifts the Γ-point degeneracy in the top of the valence band such that heavy (light) holes become the ground (excited) state, the detrimental effect from the strong spin mixing of light-hole states is mitigated. Accordingly, the typical ultrafast spin relaxation of holes in unstrained p-type semiconductors [105–107] can be dramatically suppressed when the strain-induced splitting between the heavy- and light-hole valence bands is larger than $k_B T$.

This paper is organized as follows. Section II provides a theoretical background starting with a summary of our previous findings on interaxis valley scattering in multivalley semiconductors. The second part of Sec. II contains a discussion on a compact $\mathbf{k} \cdot \mathbf{p}$ Hamiltonian whose eigenstates are used in Sec. III to derive the intra-axis spin-flip matrix elements due to scattering off impurities. To keep the discussion succinct, many technical details on the derivation of the Hamiltonian and its utilization in the context of intra-axis spin flips are provided in Appendix A. Section IV includes integration of all spin-flip processes due to electron-phonon and electron-impurity interactions, from which one can quantify the dependence of the spin relaxation on strain, temperature, donor impurity

concentration, and donor identity. Section V includes results and a discussion of these dependencies, and conclusions are provided in Sec. VI. Finally, Appendix B includes technical computational details.

II. THEORETICAL BACKGROUND

Contrary to single-valley semiconductors, such as GaAs, a zero-velocity wave packet can scatter off an impurity in multivalley semiconductors. The reason is that in addition to velocity, the wave packet has an extra "quantum number"—the valley index. We have recently shown that the spin relaxation due to scattering off impurities is governed by the interaxis valley change, while the velocity of the wave packet plays a minor role [26]. This spin-flip process is enabled by short-range interaction of the scattered electron with the spin-orbit coupling potential of the impurity. To quantify the scattering amplitude, one can make use of the analytical relation between the phase shift of scattered states and the binding energies of the impurity bound states [108–110]. This relation bypasses the need to rely on *ab initio* calculations in order to quantify the spin relaxation. Consequently, we were able to quantify the spin-flip scattering amplitude by using empirical fine-structure parameters of the impurity bound states. The spin-flip matrix element due to interaxis valley scattering off an impurity can then be written as [26]

$$M_{\rm sf} = C\pi\delta_B\Delta_{\rm so}, \qquad \delta_B = \frac{a_B^3}{V}, \tag{1}$$

where C is a constant of the order of unity that depends on spin orientation. V and a_B are the crystal volume and the electron Bohr radius, respectively. $\Delta_{\rm so}$ is the spin-splitting of the ground-state impurity level whose amplitude is commensurate with the central cell correction coming from the difference between the spin-orbit interaction of the impurity and silicon atoms, $\delta V_{\rm so}$. Because the Bohr radius is large compared with the impurity's core-region radius wherein $\delta V_{\rm so}$ is relatively strong (>1 nm versus ~0.1 nm), the central cell correction has to be strong enough in order to produce measurable spin-splitting. In other words, the strength of $\delta V_{\rm so}$ has to compensate for its short range. The dependence of $\Delta_{\rm so}$ on the difference between the spin-orbit interaction of the impurity and silicon atoms is indeed corroborated in experiments, showing that $\Delta_{\rm so}$ is of the order of 0.3, 0.1, and 0.03 meV for Sb, As, and P impurities, respectively [111,112].

To better understand the details of the impurity's spin splitting, we consider a substitutional impurity atom surrounded by four silicon atoms in a tetrahedral molecular geometry. The vast majority of shallow donors in Si are represented by such substitutional impurities whose potential has T_d point-group symmetry. Due to the valley-orbit coupling within the T_d impurity, the ground-state level $(1s)$ is split into spin-independent nondegenerate (A_1), doubly degenerate (E), and triply degenerate (T_2) states where the overall sixfold multiplicity comes from the number of conduction edge states (valley centers) [113,114]. A_1, E, and T_2 denote the symmetrized linear combinations of these valley edge states under T_d group operations. When adding the spin degree of freedom, the notable measured effect from the spin-orbit coupling is attributed to the spin splitting of the triply degenerate state (T_2)

[26,112]. This splitting is denoted by Δ_{so} in Eq. (1). We note that $\Delta_{so} = 0$ for direct-band-gap semiconductors, in which substitutional donors do not change the point-group symmetry and their ground state is nondegenerate (the conduction band has one low-energy valley in the zone center).

A. X-point k · p Hamiltonian

When the interaxis scattering is quenched by strain, various types of weak intra-axis mechanisms become relevant. Contrary to the interaxis mechanisms, the intra-axis ones depend on the velocity of the wave packet. The spin-flip dependence on the momentum of the incoming and scattered wave packets can be captured by employing a spin-dependent **k · p** Hamiltonian to describe the low-energy conduction-band states. We construct the Hamiltonian by using its invariance to the symmetry operations of the space group G_{32}^2, which describes the symmetry of the X point at the edge of the Brillouin zone in diamond crystal structures [25,115–119]. In silicon, the X point is closer to the absolute conduction-band minimum than all other high-symmetry points, thereby allowing us to reliably express the low-energy conduction states using a minimal set of basis functions [18,115]. Due to the symmetry of the crystal, only one of the six conduction-band valleys in silicon is studied, and we arbitrary identify it as the valley along the $+z$ crystallographic axis for which the X point corresponds to $\mathbf{k} = (0,0,2\pi/a)$. The results presented below can be readily extended to other valleys by cyclic coordinate permutations.

The **k · p** state expansion in the vicinity of the X point is carried by employing basis functions for the lowest pair of conduction bands and the upper pair of valence bands. Inclusion of the valence states is imperative since they bring in the mass anisotropy and spin mixing of the states [18,19,115]. The nomenclature for the irreducible representations (IRs) of the conduction and valence pairs is X_1 and X_4, respectively. Each of these IRs is two-dimensional due to the twofold band degeneracy at the X point of diamond crystal structures, originating from time-reversal and glide-reflection symmetries [25]. We denote the corresponding spinless basis states as $X_1 = (X_1^{2'}, X_1^1)$ and $X_4 = (X_4^x, X_4^y)$. The superscript indexing of the basis states is reminiscent of their compatibility relations with IRs of the Δ axis connecting the Γ and X points. Namely, $\Delta_{2'(1)}$ denotes the top (bottom) branches of the conduction band, while $\Delta_{x,y}$ denotes the degenerate valence band along the Δ axis (heavy and light holes). The compatibility relation also allows us to relate the basis functions along the Δ axis. For example, $\psi_{\Delta_{2'},k_z}(\mathbf{r}) \simeq e^{i(k_z-k_X)z}\psi_{X_1^{2'}}(\mathbf{r})$, where $k_X = 2\pi/a$. Following the notation of Ref. [115], the basis components are chosen to be complex conjugate of each other,

$$X_1^{2'*} = X_1^1, \quad X_4^{x*} = X_4^y. \tag{2}$$

While our expansion is carried around one of the equivalent X points, the eigenstates involved in an intervalley g-process can be readily connected by time-reversal and space inversion symmetries,

$$|\Uparrow\mathbf{k}\rangle = -\hat{I}|\Uparrow-\mathbf{k}\rangle, \quad |\Downarrow\mathbf{k}\rangle = -\hat{I}|\Downarrow-\mathbf{k}\rangle,$$
$$|\Downarrow\mathbf{k}\rangle = -i\hat{T}|\Uparrow-\mathbf{k}\rangle, \quad |\Uparrow\mathbf{k}\rangle = i\hat{T}|\Downarrow-\mathbf{k}\rangle. \tag{3}$$

$\hat{I}$ and $\hat{T}$ are operators of space and time reversal. These relations are derived by choosing a gauge according to which spatial inversion negates spinors, and by letting complex conjugation and spatial inversion act on the basis functions in Eq. (2) equivalently.

Adding the spin-orbit coupling at the X point, we note that the IRs of the corresponding double group cannot be factorized into a product of $\{X_1^{2'}, X_1^1, X_4^x, X_4^y\}$ and $\{\uparrow,\downarrow\}$ [18]. As a consequence, even in the absence of impurities and at $\mathbf{k} = (0,0,k_X)$, the **k · p** Hamiltonian contains nonzero interband spin-mixing terms (see Appendix A or Ref. [19]),

$$H_{cv}|_{k=0} = i\Delta_X(\rho_x \otimes \sigma_y - \rho_0 \otimes \sigma_x). \tag{4}$$

ρ_x, ρ_y, ρ_z are pseudospin Pauli matrices due to the X-point twofold band degeneracy, and $\sigma_x, \sigma_y, \sigma_z$ are the spin Pauli matrices; ρ_0 is a 2×2 orbital unity matrix. $\Delta_X \simeq 4$ meV is the finite spin-orbit coupling parameter between X_1 and X_4 [18,19]. The presence of the spin-mixing term in Eq. (4) means that fully polarized waves are not eigenstates of an impurity-free Hamiltonian. Its eigenstates are slightly spin-mixed,

$$\langle\mathbf{r}|\Uparrow\mathbf{k}\rangle = e^{i\mathbf{k}\cdot\mathbf{r}}\sum_{i=1}^{4}[\uparrow A_i(\mathbf{k}) + \downarrow B_i(\mathbf{k})]Y_i(\mathbf{r}),$$
$$\langle\mathbf{r}|\Downarrow\mathbf{k}\rangle = i\hat{I}\hat{T}\langle\mathbf{r}|\Uparrow\mathbf{k}\rangle, \tag{5}$$

where $(Y_1, Y_2, Y_3, Y_4) = (X_1^{2'}, X_1^1, X_4^x, X_4^y)$, and

$$\mathbf{A}(\mathbf{k}) = \left[0, 1, -\frac{k_x P}{E_g}, -\frac{k_y P}{E_g}\right],$$
$$\mathbf{B}(\mathbf{k}) = \left[\frac{\eta(k_x - ik_y)}{\Delta_c}, 0, -\frac{\Delta_X'}{E_g}, -\frac{i\Delta_X'}{E_g}\right],$$
$$\eta = \frac{2iP\Delta_X}{E_g}, \quad \Delta_X' = \Delta_X - \alpha k_z', \quad \Delta_c = \frac{2\hbar^2 k_0 k_z'}{m}. \tag{6}$$

$k_z' \equiv k_z - k_X$ and Δ_c are negative for the $+z$ valley. The notations of constants in Eq. (6) and their values are the same as in Ref. [19]: $E_g \simeq 4.3$ eV is the X-point band gap, $P \simeq 10$ eV $a/2\pi$ is the interband momentum matrix element, where $a = 5.43$ Å in Si, and $|\Delta_c| \simeq 0.5$ eV is the energy splitting between the top and bottom conduction bands at the valley-edge position (15% away from the X point toward the Γ point; $k_0 = 0.15k_X$). Finally, $\alpha \simeq -3.1$ meV $a/2\pi$ is a correction to the X-point spin-orbit coupling parameter (Δ_X) due to the finite distance of the valley bottom from the X point. Below, we make use of the state expansion in Eq. (6) to derive intra-axis spin-flip matrix elements.

III. SPIN-FLIP PROCESSES IN STRAINED SILICON DUE TO SCATTERING OFF IMPURITIES

A central goal of this paper is to derive intra-axis matrix elements due to scattering off impurities. These matrix elements, $M_{sf}(\mathbf{k}_i, \mathbf{k}_f) = \langle\Downarrow\mathbf{k}_f|V|\Uparrow\mathbf{k}_i\rangle$, where V is the impurity potential, govern the spin relaxation when the strain-induced valley splitting is large enough to quench interaxis scattering. For elastic scattering off impurities, $k_i = k_f$, the resulting spin

relaxation rate is [19]

$$\frac{1}{\tau_s} = \frac{4\pi N_D V}{\hbar} \left\langle \sum_{\mathbf{k}_f} |M_{\mathrm{sf}}(\mathbf{k}_i, \mathbf{k}_f)|^2 \delta\left(E_{\mathbf{k}_i} - E_{\mathbf{k}_f}\right) \right\rangle_{\mathbf{k}_i}, \quad (7)$$

where N_D is the donor impurity concentration. The average over $\mathbf{k}_i$ represents weighted integration over $\partial \mathcal{F}/\partial E_{\mathbf{k}_i}$, where $\mathcal{F}$ denotes the electron distribution function. This weighted integration is exact for any distribution in the limit of infinitesimal net-spin polarization. The prefactor of $4\pi/\hbar$ instead of $2\pi/\hbar$ denotes the fact that the net number of spin-polarized electrons changes by two with each spin flip. It is noted that only first-order processes are relevant for calculation of $M_{\mathrm{sf}}(\mathbf{k}_i, \mathbf{k}_f)$; we have found zero net contribution from second-order processes in which an electron undergoes intra-axis scattering via two virtual elementary interaxis scattering events.

We consider three types of spin-flip processes due to intra-axis scattering. Two of the three are Elliott processes in which the spin flip is governed by the spin-orbit coupling of the host crystal, whereas the scattering potential is spin-independent [101,120]. One Elliott process involves long-range interaction with the ionized-impurity potential, and the second one is a central cell correction coming from short-range interaction with the spin-independent part of the impurity potential. Using the $\mathbf{k} \cdot \mathbf{p}$ expansion in Eq. (6), an Elliott spin-flip matrix element has the form

$$M_{\mathrm{sf}}^{E,i}(\mathbf{k}_i, \mathbf{k}_f) \simeq \mathbf{A}^T(\mathbf{k}_f)\mathcal{H}_E \mathbf{B}(\mathbf{k}_i) - \mathbf{B}^T(\mathbf{k}_f)\mathcal{H}_E \mathbf{A}(\mathbf{k}_i), \quad (8a)$$

$$M_{\mathrm{sf}}^{E,g}(\mathbf{k}_i, \mathbf{k}_f) \simeq \mathbf{A}^T(\mathbf{k}_f)\mathcal{H}_E \tilde{\mathbf{B}}(\mathbf{k}_i) - \mathbf{B}^T(\mathbf{k}_f)\mathcal{H}_E \tilde{\mathbf{A}}(\mathbf{k}_i), \quad (8b)$$

for the intravalley and intervalley g-process, respectively. $\mathcal{H}_E$ is a 4×4 interaction matrix whose form will be deduced from the symmetry of the spin-independent potential. Following Eqs. (2) and (3), $\tilde{\mathbf{A}}$ and $\tilde{\mathbf{B}}$ in the g-process matrix element are found by exchanging the coefficients of $X_1^{2'}$ and X_1^1 as well as of X_4^x and X_4^y in Eq. (6).

The last intra-axis scattering that we will consider in this work is a Yafet process in which the spin flip is governed by the spin-orbit coupling of the scattering potential [20,101]. Although much weaker than the dominant interaxis Yafet mechanism, both originate from short-range interaction with the spin-orbit coupling of the impurity. The spin-flip matrix elements have the form

$$M_{\mathrm{sf}}^{Y,i}(\mathbf{k}_i, \mathbf{k}_f) \simeq \mathbf{A}^T(\mathbf{k}_f)\mathcal{H}_Y \mathbf{A}(\mathbf{k}_i), \quad (9a)$$

$$M_{\mathrm{sf}}^{Y,g}(\mathbf{k}_i, \mathbf{k}_f) \simeq \mathbf{A}^T(\mathbf{k}_f)\mathcal{H}_Y \tilde{\mathbf{A}}(\mathbf{k}_i), \quad (9b)$$

where we have neglected the contribution from the cross products of $\mathbf{B}$ vectors due to the smallness of the spin-orbit coupling in silicon. It is noted that Elliott and Yafet matrix elements can become comparable if the smallness of the nonzero elements in $\mathbf{B}$ (compared with those in $\mathbf{A}$) is compensated for by the smallness of the elements in $\mathcal{H}_Y$ (compared with those in $\mathcal{H}_E$). In fact, this scenario applies in the case of the electron-phonon interaction for which the spin-orbit coupling of the host atoms drives both $\mathbf{B}$ and $\mathcal{H}_Y$ [19].

A. Long-range Coulomb potential (Elliott)

We first consider electron scattering off the long-range Coulomb potential of ionized donor impurities,

$$V(\mathbf{r}) = \frac{4\pi e^2}{\epsilon r} e^{-\kappa r}, \qquad \kappa = \sqrt{\frac{4\pi e^2 N_D}{\epsilon k_B T}}, \quad (10)$$

where κ is the Thomas-Fermi screening wave number, e is the electron charge, and ϵ is the dielectric constant. The long-range nature of this scattering stems from the fact that the screened Coulomb potential decays on a length scale much longer than the lattice constant, $\kappa a \ll 1$. We note that while scattering off this potential dominates momentum relaxation in highly doped silicon [24], its role in the context of spin relaxation is marginal compared with the interaxis short-range scattering in unstrained silicon [26]. The long-range and radial symmetry of the screened potential allows us to consider $\mathcal{H}_E$ as a product of the unity matrix with the Fourier transform of the screened Coulomb potential,

$$\mathcal{H}_E = V_s(\mathbf{q})\mathbb{1}, \qquad V_s(\mathbf{q}) = \frac{4\pi e^2}{\epsilon V(q^2 + \kappa^2)}, \quad (11)$$

where $\mathbf{q} = \mathbf{k}_i - \mathbf{k}_f$. Substituting Eqs. (11) and (6) in (8a), we find the long-range intravalley spin-flip matrix element,

$$M_{E,i}^{\mathrm{lr}}(\mathbf{k}_i, \mathbf{k}_f) = \frac{\Delta_X' P}{E_g^2}(k_{+,i} - k_{+,f})V_s(\mathbf{q}), \quad (12a)$$

where $k_{+,i(f)} = k_{x,i(f)} + i k_{y,i(f)}$. Similarly, the spin-flip matrix element for the intervalley g-process is found by substituting Eqs. (11) and (6) in (8b),

$$M_{E,g}^{\mathrm{lr}}(\mathbf{k}_i, \mathbf{k}_f) = \frac{\Delta_X' P}{E_g^2}(k_{-,i} + k_{-,f})V_s(\mathbf{q}_g + \mathbf{q}), \quad (12b)$$

where $k_{-,i(f)} = k_{x,i(f)} - i k_{y,i(f)}$ and $\mathbf{q}_g = 0.3\mathbf{k}_X$. The long-range nature of the Coulomb potential renders the intravalley process much stronger, $V_s(\mathbf{q} \to 0) \gg V_s(\mathbf{q}_g)$.

B. Spin-orbit coupling of impurities (Yafet)

The second spin-flip process we consider is due to the spin-orbit coupling of the donor impurities. Their presence lowers the diamond point-group symmetry from $\hat{I} \otimes T_d$ to T_d. Inspecting the symmetry operations of the space group G_{32}^2, we identify M_2' as the IR that can represent the lowered symmetry of the impurity potential. Compared with the identity IR (M_1) whose characters are all "1," the characters of M_2' are negated for all symmetry operations that involve exchanging the two atoms in the unit cell. As elaborated on in Appendix A 4, the form of $\mathcal{H}_Y$ in Eq. (9) is extracted from the following considerations. First, we identify the selection rules of M_2' with IRs whose transformation properties match those of transverse vector components (such as k_x and k_y) and transverse pseudovector components (such as σ_x and σ_y). These IRs are represented by M_5 and M_5', respectively, where the selection rules follow,

$$M_2' \otimes M_5 = M_5', \qquad M_2' \otimes M_5' = M_5. \quad (13)$$

That is, coupling to the impurities transforms a vector-type interaction to a pseudovector one and vice versa. Next, we

use these selection rules to construct $\mathcal{H}_Y$ due to the presence of impurities. Specifically, we look for terms that stem from the coupling between valence and conduction states since this coupling corresponds to transverse vector and pseudovector terms in the Hamiltonian ($X_1 \otimes X_4 = M_5 \oplus M_5'$). For the Yafet process, $\mathcal{H}_Y$ is constructed by replacing the $\mathbf{k}_{x,y}$ terms with $\sigma_{x,y}$ alongside a replacement of crystal parameters with impurity ones (e.g., $Pk_i \to \delta_B \Delta_{\text{so}}$). Using this procedure, the leading Yafet term has the form (Appendix A 4)

$$\mathcal{H}_Y = -i\delta_B \Delta_{\text{so}}(\rho_y \otimes \sigma_x + i\rho_z \otimes \sigma_y). \tag{14}$$

Substituting Eqs. (14) and (6) in (9), we find the intravalley and g-process spin-flip matrix elements

$$M_{Y,i}(\mathbf{k}_i, \mathbf{k}_f) = \frac{\delta_B \Delta_{\text{so}} P}{E_g}(k_{-,i} + k_{-,f}), \tag{15a}$$

$$M_{Y,g}(\mathbf{k}_i, \mathbf{k}_f) = i\frac{\delta_B \Delta_{\text{so}} P}{E_g}(k_{+,i} + k_{+,f}). \tag{15b}$$

C. Central cell Elliott spin flip

The final spin-flip process we consider is governed by the spin-orbit coupling of the host crystal (silicon atoms), and it takes place when electrons are scattered off the short-range and spin-independent part of the impurity potential. To derive the form of the resulting Elliott matrix, $\mathcal{H}_E$, we inspect the coupling within conduction-band basis states (the conduction-valence coupling gives rise to the Yafet process, as discussed in the previous section). The selection rule for coupling between conduction states follows from

$$X_1 \otimes X_1 = M_1 \oplus M_2' \oplus M_3' \oplus M_4. \tag{16}$$

Relevant to our study are M_2' and the identity IR M_1. The identity IR represents the radial part of the central cell correction, and as such it gives rise to diagonal coupling between X_1^1 states or between $X_1^{2'}$ states. On the other hand, M_2' represents the lowered symmetry part of the impurity potential. Its transformation properties give rise to off-diagonal coupling between X_1^1 and $X_1^{2'}$ states [19]. We therefore have two terms in the short-range Elliott matrix,

$$\delta H_c = \delta_B \Delta_0 \rho_0 \otimes \sigma_0 + \delta_B \Delta_1 \rho_y \otimes \sigma_0, \tag{17}$$

where σ_0 is a 2×2 unity matrix acting in spinor space, and Δ_0 and Δ_1 are the diagonal and off-diagonal scattering constants. To estimate their values, we make use of the fact that the short-range and spin-independent part of the impurity potential splits the sixfold-degenerate ground-state energy due to valley-orbit coupling [113]. Similar to the Yafet process for which the scattering amplitude was estimated from Δ_{so} (the spin-splitting of T_2 due to the spin-orbit coupling of the impurity), the values of Δ_0 and Δ_1 can be uniquely determined via the empirically known spin-independent binding energies of the ground state (A_1, E, and T). Below we use $\Delta_0 \simeq 4$ meV and $\Delta_1 \simeq 1.5$ meV following the work of Friesen, who studied the Stark effect for donors in silicon [121]. Contrary to Δ_{so}, the values of Δ_0 and Δ_1 are largely insensitive to the identity of the substitutional donor (Sb, As, and P) [114,122].

Substituting Eqs. (17) and (6) in (8), we find the short-range intravalley and g-process spin-flip matrix elements

$$M_{E,i}^{\text{sr}}(\mathbf{k}_i, \mathbf{k}_f) = i\frac{\delta_B \Delta_1 \eta}{4\Delta_c}(k_{+,i} + k_{+,f}), \tag{18a}$$

$$M_{E,g}^{\text{sr}}(\mathbf{k}_i, \mathbf{k}_f) = -\frac{\delta_B \Delta_0 \eta}{4\Delta_c}(k_{+,i} + k_{+,f}). \tag{18b}$$

D. Total intra-axis spin-flip matrix elements

The total matrix element is denoted by the sum of Eqs. (12), (15), and (18). For spin flips due to the intravalley and g-process, one gets

$$M_i(\mathbf{k}_i, \mathbf{k}_f) \simeq \frac{P}{E_g}\delta_B \Delta_{\text{so}}(k_- + C_{\mathbf{q}}q_+ + D_1 k_+), \tag{19a}$$

$$M_g(\mathbf{k}_i, \mathbf{k}_f) \simeq \frac{iP}{E_g}\delta_B \Delta_{\text{so}}(k_- + C_{\mathbf{q}_g}q_- - D_0 k_+), \tag{19b}$$

where $k_\pm = k_{\pm,i} + k_{\pm,f}$, $q_\pm = k_{\pm,i} - k_{\pm,f}$, and

$$C_{\mathbf{p}} = \frac{V_s(\mathbf{p})\Delta_X'}{\delta_B E_g \Delta_{\text{so}}}, \qquad D_{1(0)} = \frac{2\Delta_{1(0)}\Delta_X}{\Delta_c \Delta_{\text{so}}}. \tag{19c}$$

The C and D terms represent the long- and short-range Elliott processes, respectively. For Si:Sb in which the spin-orbit coupling of the impurity is relatively strong ($\Delta_{\text{so}} \simeq 0.3$ meV) [111,112], both Elliott processes can be neglected and the spin relaxation is governed by the Yafet process ($C, D \ll 1$). Only for the case of Si:P ($\Delta_{\text{so}} \simeq 0.03$ meV) [112] do the Elliott processes become comparable to the Yafet process. This result is not surprising given that the spin-orbit coupling of silicon is smaller than that of antimony and arsenic while being comparable to that of phosphorus. In addition, we can quantify the ratio between intra-axis and interaxis spin-flip matrix elements in unstrained silicon by comparing Eqs. (19) and (1). Using the facts that in semiconductors $P/E_g \sim a/2\pi$ and $k^2 \sim 2mk_B T/\hbar^2$, the ratio is of the order of $2mk_B T a^2/h^2$, revealing that the intra-axis spin-flip matrix element is about three orders of magnitude weaker than the interaxis one at room temperature (and more than that at lower temperatures).

Finally, we remark on the qualitative difference between spin flips caused by electron-phonon and electron-impurity interactions. In the case of phonons, the spin-orbit coupling of the host crystal drives both the Elliott and Yafet processes, giving rise to the cancellation of the leading Elliott and Yafet intravalley processes when space inversion symmetry is respected [19,20]. Yafet found that in silicon this cancellation gives rise to a quadratic rather than a linear dependence of the intravalley spin-flip matrix element on the transverse components of the acoustic-phonon wave vector, ($\propto q_\pm^2$) [20]. On the other hand, the intra-axis spin-flip matrix elements due to scattering off impurities have a linear dependence on the transverse crystal momentum of the initial and final states, as shown in Eq. (19). The reason for the linear dependence is that there is no Elliott-Yafet cancellation when dealing with impurities, whose presence breaks the space inversion symmetry and whose spin-orbit coupling is not related to that of the host-crystal atoms. Quantitatively, this difference can be seen from the lack of interference terms between the short-range Yafet, short-range Elliott, and long-range Elliott

processes after averaging the value of $|M_{i/g}(\mathbf{k}_i, \mathbf{k}_f)|^2$ over angular angles.

IV. ANISOTROPY AND OVERALL SPIN RELAXATION IN STRAINED SILICON

So far, we have assumed spin orientation along the valley axis, $\mathbf{s} \parallel \mathbf{z}$. The matrix elements for arbitrary orientation, $\mathbf{s} \not\parallel \mathbf{z}$, can be related with those in Eq. (19) by [19]

$$\langle \Uparrow_{\mathbf{s}} \mathbf{k}_f | V | \Downarrow_{\mathbf{s}} \mathbf{k}_i \rangle = \cos^2 \frac{\theta}{2} e^{i\phi} \langle \Uparrow_{\mathbf{z}} \mathbf{k}_f | V | \Downarrow_{\mathbf{z}} \mathbf{k}_i \rangle$$
$$- \sin^2 \frac{\theta}{2} e^{-i\phi} \langle \Downarrow_{\mathbf{z}} \mathbf{k}_f | V | \Uparrow_{\mathbf{z}} \mathbf{k}_i \rangle, \quad (20)$$

where θ is measured from the valley axis and ϕ is the azimuthal angle. We have omitted terms proportional to $\langle \Downarrow_{\mathbf{z}} \mathbf{k}_f | V | \Downarrow_z \mathbf{k}_i \rangle - \langle \Uparrow_{\mathbf{z}} \mathbf{k}_f | V | \Uparrow_z \mathbf{k}_i \rangle$ since they vanish identically for linear-in-$\mathbf{k}$ terms in Eq. (19). Similar to the case of phonon-induced spin relaxation [19], summing the contributions from all six valleys in unstrained silicon yields isotropic spin relaxation. The anisotropy emerges when applying strain, yielding twice as strong intra-axis spin relaxation when the low-energy valley pair and spin orientation are collinear compared with the perpendicular case.

The total spin relaxation rate is the sum of the intervalley f-process (interaxis scattering), the intravalley process, and the intervalley g-process (intra-axis scattering),

$$\frac{1}{\tau_s} = \frac{1}{\tau_s^{\text{inter}}} + \frac{1}{\tau_s^{\text{intra}}}. \quad (21)$$

The effect of compressive strain on the intra-axis and interaxis processes is different since only the latter can be completely quenched when the valley splitting energy is large: $1/\tau_s^{\text{inter}} \to 0$ when $e^{-\Delta_v/k_B T} \ll 1$, where Δ_v is the strain-induced valley splitting energy. On the other hand, the intra-axis relaxation rate, $1/\tau_s^{\text{intra}}$, is only mildly affected via the emerged anisotropy. Below we focus on the two extreme cases for parallel and perpendicular orientations of strain and spin axes, and we express the total spin relaxation in silicon due to electron-impurity and electron-phonon interactions as functions of temperature, donor concentration, and valley splitting energy (for uniaxial compressive strain along one of the equivalent [001]-crystallographic directions).

A. Total interaxis spin relaxation (f-process)

The f-process spin relaxation is expressed by

$$\frac{1}{\tau_s^{\text{inter}}} = \frac{C_{I,f}}{\tau_{I,f}} + \sum_{j=1,2,3} \frac{C_{\Sigma_j}}{\tau_{\Sigma_j}}, \quad (22)$$

where the first term denotes the contribution due to scattering off impurities [26], and the sum denotes the contribution from the three Σ-axis phonon modes that govern the spin-flip f-process intervalley scattering [19]. The τ terms on the right-hand side denote the corresponding strain-free spin relaxation when assuming electron Boltzmann distribution in Eq. (7). $C_{I,f}$ and C_{Σ_j} denote correction factors caused by the strain suppression of the f-process (both approach zero when $e^{-\Delta_v/k_B T} \ll 1$), as well as the correction to the spin relaxation when deviating from the Boltzmann limit (high density and

low temperature). The electron-impurity spin relaxation rate constant in (22) follows,

$$\frac{1}{\tau_{I,f}} = \frac{N_D a_B^3}{\tau_D} \sqrt{\frac{T}{T_R}}, \qquad \frac{1}{\tau_D} = \frac{16\sqrt{\pi}}{3\hbar} \frac{\Delta_{\text{so}}^2}{E_R}. \quad (23)$$

$E_R = k_B T_R = \hbar^2/2m_d a_B^2 \sim 35$ meV is the effective Rydberg energy in silicon, where $m_d = 0.32 m_0$ is the effective density-of-state mass and $a_B \simeq 1.85$ nm. The value of τ_D is about 30 ps for Sb, 240 ps for As, and 3 ns for P. The electron-impurity correction factor in Eq. (22) is expressed by

$$C_{I,f} = \frac{3}{4} \frac{(1 + \delta_{s,v}) \mathcal{I}_f(\Delta_v, \Delta_v) + (3 - \delta_{s,v}) \mathcal{I}_f(\Delta_v, 0)}{\mathcal{I}_1(0) + 2\mathcal{I}_1(\Delta_v)}. \quad (24)$$

$\delta_{s,v} = 1(0)$ if the spin orientation is collinear (perpendicular) to the low-energy valley axis. The other terms are defined by the following two integrals:

$$\mathcal{I}_f(\varepsilon_1, \varepsilon_2) = \int_{\varepsilon_m}^{\infty} d\varepsilon \frac{\sqrt{(\varepsilon - \varepsilon_1)(\varepsilon - \varepsilon_2)}}{k_B T} \frac{\partial \mathcal{F}}{\partial \varepsilon}, \quad (25)$$

where $\varepsilon_m = \max\{\varepsilon_1, \varepsilon_2\}$, and

$$\mathcal{I}_n(\varepsilon_1) = \frac{2}{\sqrt{\pi}} \int_{\varepsilon_1}^{\infty} d\varepsilon \left(\frac{\varepsilon - \varepsilon_1}{k_B T} \right)^{n/2} \frac{\partial \mathcal{F}}{\partial \varepsilon}. \quad (26)$$

In the following, we will show results when using the Fermi-Dirac distribution to represent $\mathcal{F}(\varepsilon)$. In the Boltzmann limit where $\max\{\mathcal{F}(\varepsilon)\} \ll 1$, both integrations can be performed analytically yielding $\mathcal{I}_1(\varepsilon_1) \to e^{-\varepsilon_1/k_B T}$ and $\mathcal{I}_f(\varepsilon_1, \varepsilon_2) \to r_d e^{-r_a} K_1(r_d)$, where $r_d = |\varepsilon_2 - \varepsilon_1|/2k_B T$, $r_a = (\varepsilon_2 + \varepsilon_1)/2k_B T$, and K_1 is the first-order modified Bessel function of the second kind. Figure 2(a) shows the value of $C_{I,f}$ at 77 K (dashed lines) and 300 K (solid lines) as a function
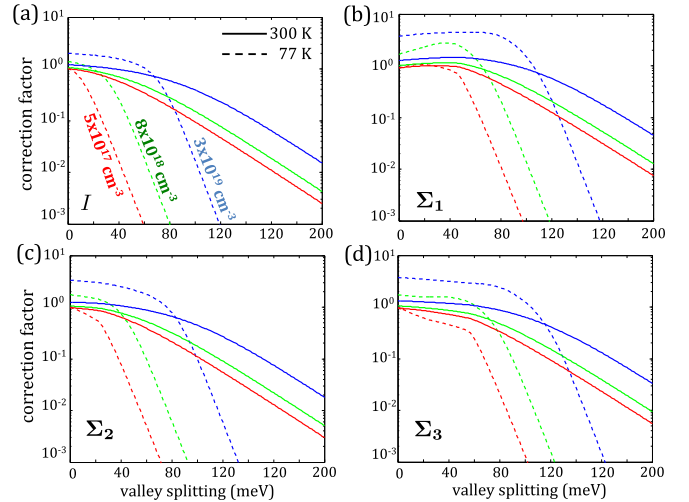

FIG. 2. Correction factors of the intervalley f-process as a function of the strain-induced valley splitting energy. The solid (dashed) lines show room-temperature (77 K) results for three different densities (5×10^{17}, 8×10^{18}, and 3×10^{19} cm^{-3}). The electron-impurity correction factor is shown in (a), and the electron-phonon correction factors are shown in (b)–(d) for each of the three symmetry-allowed phonons modes (Σ_{1-3}). All of the results are shown for a parallel configuration between the strain and spin orientation axes. The results for the perpendicular configuration are similar in nature.

of valley splitting for three donor densities. The value of $C_{I,f}$ at zero strain approaches unity at low densities.

The f-process spin relaxation in Eq. (22) due to electron-phonon interaction is decomposed in a similar way. The rate constants denote the corresponding strain-free spin relaxation in the Boltzmann limit [19],

$$\frac{1}{\tau_{\Sigma_j}} = \frac{\sqrt{r_j}}{\tau_j} \frac{K_1(r_j)}{\sinh(r_j)}. \tag{27}$$

The temperature dependence is carried by the parameter $r_j = T_j/2T$, where $T_1 = 540$ K, $T_2 = 660$ K, and $T_3 = 270$ K are the energies of the three types of symmetry-allowed shortwave phonon modes, Σ_{1-3}. The time constants τ_j are governed by the corresponding electron-phonon spin-flip matrix elements [19], yielding $\tau_1 \sim 20$ ns, $\tau_2 \sim 70$ ns, and $\tau_3 \sim 200$ ns. The expressions for the phonon-related strain suppression factors are cumbersome [C_{Σ_j} in Eq. (22)], and we present them in Appendix B. Their dependence on the strain-induced valley splitting energy is shown in Figs. 2(b)–2(d).

B. Total intra-axis spin relaxation

The spin relaxation rate due to intravalley and intervalley g-processes in Eq. (21) has four contributions,

$$\frac{1}{\tau_s^{\text{intra}}} = \frac{C_{I,\text{sr}}}{\tau_{I,\text{sr}}} + \frac{C_{I,\text{lr}}}{\tau_{I,\text{lr}}} + \frac{C_{\text{ac}}}{\tau_{\text{ac}}} + \frac{C_\Delta}{\tau_\Delta}. \tag{28}$$

The τ terms on the right-hand side are spin relaxation times when assuming electron Boltzmann distribution in unstrained silicon. The C terms are corrections due to the strain and/or deviations from Boltzmann statistics. The first term on the right-hand side denotes the contribution from electron scattering off the short-range impurity potential. Qualitatively, this mechanism influences the intravalley and intervalley g-process similarly. The second term denotes the contribution from electron scattering off the ionized impurity potential. As mentioned at the end of Sec. III A, the effect of this long-range scattering potential on the intervalley g-process is negligible compared with the intravalley one. The third and fourth terms denote contributions from electron interaction with long-wavelength acoustic phonons (intravalley) and Δ-axis shortwave phonons (intervalley g-process). We recall that a major difference from the interaxis case is that the intra-axis relaxation does not change appreciably when the valley-splitting energy is large. Here, the intra-axis C terms only bring out the anisotropy in spin relaxation; they do not become negligible at large strain levels.

Starting with the intra-axis electron-impurity processes, we calculate the resulting spin relaxation by substituting Eq. (19) into (7). For the short-range interaction, denoted by the first term in Eq. (28), we get that the spin relaxation in the Boltzmann limit yields

$$\frac{1}{\tau_{I,\text{sr}}} = \alpha_D \frac{N_D a_B^3}{\tau_D} \left(\frac{T}{T_R}\right)^{\frac{3}{2}}, \quad \alpha_D = \frac{(4 + 2D_0^2 + 2D_1^2)P^2}{3\pi^2 a_B^2 E_g^2}, \tag{29}$$

where τ_D and T_R were defined in Eq. (23), and $D_{0,1}$ was defined in Eq. (19c). Compared with τ_D, α_D has a weaker dependence on donor identity, ranging from 1.6×10^{-3} for Si:Sb and $5.7 \times$

10^{-3} for Si:P. Compared with the impurity-induced interaxis spin relaxation in Eq. (23), the smallness of α_D demonstrates the negligible effect of the intra-axis impurity scattering on spin relaxation in unstrained silicon. When deviating from the Boltzmann limit, the strain-dependent correction factor in Eq. (28) follows,

$$C_{I,\text{sr}} = \frac{3\sqrt{\pi}}{16} \frac{(1 + \delta_{s,v})\mathcal{I}_4(0) + (3 - \delta_{s,v})\mathcal{I}_4(\Delta_v)}{\mathcal{I}_1(0) + 2\mathcal{I}_1(\Delta_v)}, \tag{30}$$

where $\mathcal{I}_n(\varepsilon)$ was defined in Eq. (26). Turning to the long-range interaction, denoted by the second term in Eq. (28), we get that the spin relaxation in unstrained silicon in the Boltzmann limit yields

$$\frac{1}{\tau_{I,\text{lr}}} = \frac{N_D a_B^3}{\tau_{\text{lr},0}} \sqrt{\frac{T_R}{T}} \mathcal{L}(r_N), \tag{31a}$$

where $r_N = N_D/N_T$ and

$$\tau_{\text{lr},0} = \frac{9\hbar a_B^2 E_g^4}{128\sqrt{\pi} P^2 E_R \Delta_X^2} \approx 75 \text{ ns}, \tag{31b}$$

$$N_T = \frac{2\epsilon m_d (k_B T)^2}{\pi e^2 \hbar^2} \simeq 1.45 \times 10^{19} \left(\frac{T}{300}\right)^2 \text{ cm}^{-3}, \tag{31c}$$

$$\mathcal{L}(x) = -1 - (1 + x)e^x E_i(-x). \tag{31d}$$

Here, $E_i(x)$ is the exponential integral special function, $-E_i(-x) = \int_x^\infty dt\, e^t/t$ for $x > 0$. Unlike the short-range mechanism, there is no dependence on donor identity (all donors yield similar long-range ionized Coulomb potential). Similar to the other intra-axis mechanisms, however, this mechanism has a negligible contribution to the spin relaxation in unstrained silicon compared with the contribution from the interaxis processes. In fact, it will be shown to be smaller than the intra-axis electron-phonon interaction as well as the intra-axis short-range impurity scattering in Si:Sb and Si:As. Following the notation used in Eq. (28), the strain-dependent correction factor when deviating from the Boltzmann limit is

$$C_{I,\text{lr}} = \frac{3\sqrt{\pi}}{8\mathcal{L}(r_N)} \frac{(1 + \delta_{s,v})\mathcal{I}_{\text{lr}}(0) + (3 - \delta_{s,v})\mathcal{I}_{\text{lr}}(\Delta_v)}{\mathcal{I}_1(0) + 2\mathcal{I}_1(\Delta_v)}, \tag{32a}$$

where

$$\mathcal{I}_{\text{lr}}(\varepsilon_0) = \int_{\varepsilon_0}^\infty d\varepsilon \frac{\partial \mathcal{F}}{\partial \varepsilon} \left(\ln\left(1 + G_{\varepsilon,\varepsilon_0}\right) - \frac{G_{\varepsilon,\varepsilon_0}}{1 + G_{\varepsilon,\varepsilon_0}} \right),$$

$$G_{\varepsilon,\varepsilon_0} = \frac{1}{r_N} \frac{\varepsilon - \varepsilon_0}{k_B T}. \tag{32b}$$

The final spin relaxation mechanisms are those from intra-axis electron-phonon scattering, denoted by the last two terms in Eq. (28). They are driven by intravalley scattering with acoustic phonons (mainly transverse modes) and g-process intervalley scattering with shortwave phonon modes of Δ_1 symmetry [19]. The intravalley and intervalley g-process strain-free rates in the Boltzmann limit follow [18,19],

$$\frac{1}{\tau_{\text{ac}}} = \frac{1}{\tau_{\text{ac},0}} \left(\frac{T}{T_R}\right)^{5/2}, \qquad \frac{1}{\tau_\Delta} = \frac{\sqrt{r_g}}{\tau_{\Delta,0}} \frac{K_2(r_g)}{\sinh(r_g)}, \tag{33}$$

where $\tau_{\text{ac},0} \sim 50$ ns and $\tau_{\Delta,0} \sim 2$ μs are governed by the respective electron-phonon spin-flip matrix elements. The
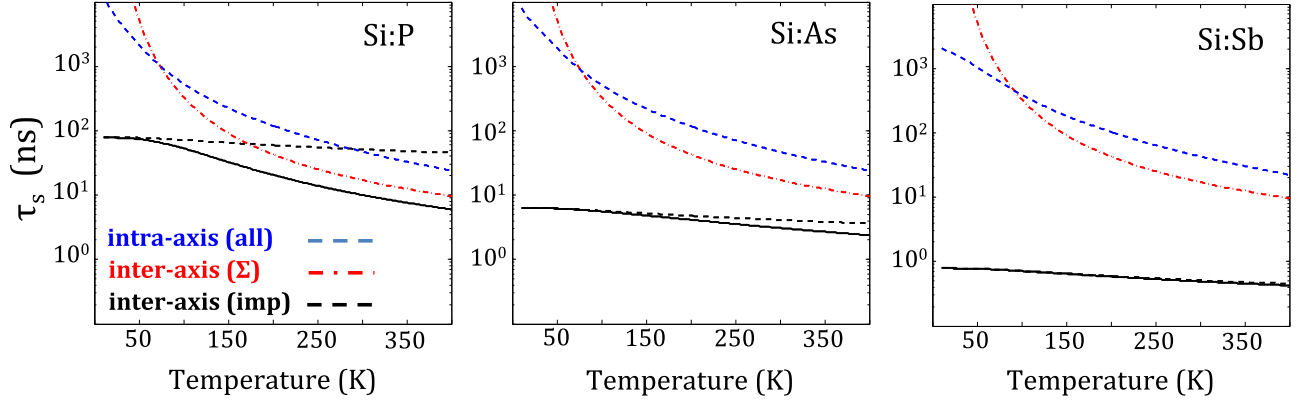
FIG. 3. Spin relaxation in unstrained n-type silicon doped with P (left), As (middle), and Sb (right) as a function of temperature. The donor concentration is $N_D = 10^{19}$ cm^{-3}. The solid black lines denote the total relaxation time. The interaxis mechanisms from phonons and impurities are shown by the dotted-dashed red lines and dashed black lines, respectively. The intra-axis mechanism is shown by the dashed blue line, and it includes contributions from both phonons and impurities.

temperature dependence of the g-process is carried by the parameter $r_g = T_g/2T$, where $T_g = 240$ K is the energy of the relevant Δ_1 shortwave phonon mode. K_2 is the second-order modified Bessel function of the second kind. The intravalley correction factor is similar to that of the short-range potential, $C_{ac} = C_{I,sr}$, provided in Eq. (30). The expression for the intervalley g-process correction is cumbersome (C_Δ), and we provide it in Appendix B. In the Boltzmann limit, all of the intra-axis correction factors approach

$$\begin{aligned} C_{I,sr}, \quad C_{I,lr}, \\ C_{ac}, \quad C_\Delta, \end{aligned} \rightarrow \frac{3}{4}\left[1 + \frac{e^{-2r_v} + \delta_{s,v}(1 - e^{-2r_v})}{1 + 2e^{-2r_v}}\right], \quad (34)$$

where $r_v = \Delta_v/2k_BT$. In this limit and for large valley-splitting energy ($e^{-2r_v} \ll 1$), the intra-axis spin relaxation is twice as strong when the strain and spin orientations are parallel ($\delta_{s,v} = 1$) compared with the case in which they are perpendicular ($\delta_{s,v} = 0$).

V. RESULTS AND DISCUSSION

The analysis provided in the previous section allows us to quantify the spin relaxation time of mobile electrons in n-type silicon for any temperature, donor concentration,

donor identity, and valley splitting energy (at the uniaxial compressive strain configuration). It takes less than a minute to generate the results of each of the figures in this work with a simple computer.

Figure 3 shows the spin relaxation times in unstrained silicon as a function of temperature in Si:P, Si:As, and Si:Sb. The donor concentration in all cases is $N_D = 10^{19}$ cm^{-3}. For the case of Si:Sb, shown in the right panel, the relaxation is governed by interaxis scattering off impurities at all temperatures [26]. In Si:P, the spin relaxation is governed by this mechanism at low temperatures and by the other interaxis mechanism at high temperatures (interaction with shortwave Σ-axis phonons). The intra-axis spin relaxation (τ_s^{intra}), shown by the dashed-blue line, has a marginal contribution at all cases. The small effect of the intra-axis mechanism applies at lower donor concentrations as well, in which the relaxation is largely governed by the interaction with the shortwave Σ-axis phonons [18]. The only means to bring the intra-axis mechanism into play is by strain-induced quenching of the interaxis mechanisms.

Figure 4 shows the spin relaxation time as a function of the strain-induced valley splitting energy in Si:P, Si:As, and
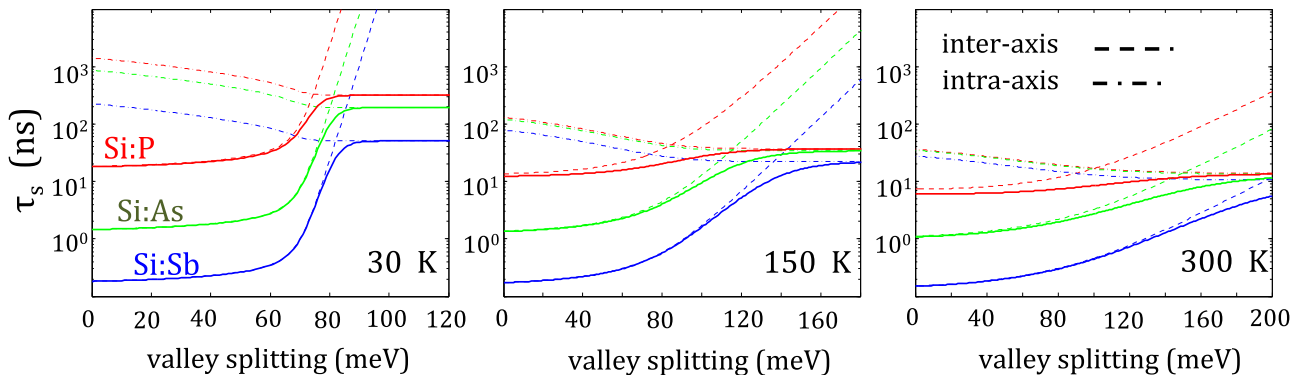

FIG. 4. Spin relaxation in silicon as a function of strain-induced valley splitting energy at 30 K (left), 150 K (middle), and 300 K (right). The donor concentration is $N_D = 3 \times 10^{19}$ cm^{-3}, and the strain axis is parallel to the spin orientation ($\delta_{s,v} = 1$). The solid lines denote the total relaxation time. The interaxis and intra-axis contributions are denoted by the dashed and dotted-dashed lines, respectively.

Si:Sb at three temperatures. The donor concentration in all cases is $N_D = 3 \times 10^{19}$ cm^{-3}. In all cases, the spin relaxation is switched from being governed by interaxis mechanisms to intra-axis ones at large valley splitting energies. The enhancement in spin relaxation time is most evident at low temperatures because of the increased ratio between valley splitting and thermal energies as well as the weaker effect from phonon-related interactions. Furthermore, the improvement is larger than two orders of magnitude for Si:Sb at low temperatures due to quenching of its strong interaxis impurity scattering [26]. We also notice that while the interaxis spin relaxation mechanisms are quenched by strain, the intra-axis spin relaxation time becomes slightly faster. The latter is explained by the increase of the chemical potential with respect to the conduction-band edge. Specifically, the electron density is redistributed among six valleys at zero-strain condition while only among two valleys when the strain-induced valley splitting energy is very large. This electron redistribution leads to a change in the chemical potential, which for degenerate doping such as the one studied here, $N_D = 3 \times 10^{19}$ cm^{-3}, results in an increase from about 12 to 60 meV at room temperature (with respect to the conduction-band edge) and from about 30 to 60 meV at 30 K. Given that the intra-axis spin-flip matrix elements are commensurate with the electron wave vector, the relaxation rate increases nearly linearly with the Fermi energy.

Figure 5 shows the improvement ratio in the total spin relaxation time when the strain-induced valley splitting energy is 100 meV [i.e., $\tau_s(\Delta_v = 100 \text{ meV})/\tau_s(\Delta_v = 0 \text{ meV})$]. There are several notable features. The first one is that the improvement is mostly significant at low temperatures due to the negligible population of the high-energy valleys. At room temperature, on the other hand, $\Delta_v/k_B T$ is of the order of 4, which is not sufficient to quench the interaxis processes. Accordingly, the improvement is nearly three orders of magnitude in Si:Sb at 30 K while being much smaller at room temperature. The second feature is that the ratio initially increases with donor density before sharply decaying at very large densities. The conjunction of two factors gives rise to the initial increase: (i) the electron-impurity scattering

becomes more significant when increasing the donor density, and (ii) the strain quenches the interaxis elastic scattering more effectively than the inelastic one. The latter involves Σ-axis phonons whose energy renders the effective valley splitting smaller. Specifically, electron transitions can take place already when the electron energy is $\Delta_v - \varepsilon_\Sigma$ with respect to the conduction-band edge ($\varepsilon_\Sigma \sim 47$ meV for the dominant Σ_1 mode). As a result, the strain quenches more effectively the elastic electron-impurity interaxis mechanism for which electron transitions can take place when their energy is Δ_v. This behavior explains the initial increase of the ratio in Fig. 5 with donor concentration (the bigger role played by the electron-impurity interaction). This behavior supports the fact that the improvement is larger for Si:Sb, in which the interaxis electron-impurity scattering is strongest (compared with Si:P, in which the electron-phonon interaction plays a bigger role). Finally, the improvement in spin relaxation sharply decays for all donor types for concentrations close to $N_D = 5 \times 10^{19}$ cm^{-3}. At these densities, the chemical potential is higher than the valley splitting energy ($\mu > \Delta_v = 100$ meV in this case), so that the high-energy valleys become populated and the interaxis mechanisms are restored. In other words, the improvement in spin relaxation for degenerate doping conditions is viable when $(\Delta_v - \mu)/k_B T \gg 1$ rather than $\Delta_v/k_B T \gg 1$.

The last effect we focus on is the relative role of the intra-axis mechanisms in strained silicon. Figures 6(a) and 6(b) show the dependencies of these mechanisms on temperature and donor concentrations, respectively. The strain-induced spin splitting is $\Delta_v = 120$ meV. We notice that the spin relaxation due to the long-range interaction of electrons with impurities is a relatively weak effect (dashed lines). This interaction shows a relatively strong dependence on temperature compared with that of the short-range interaction. The reason originates from the decreased role of screening at high temperatures; thermally agitated electrons screen less effectively and therefore spin relaxation is enhanced. Finally, Fig. 6(b) shows an atypical trend wherein the intra-axis spin relaxation time due to phonons has a stronger dependence on donor density compared with the long-range interaction with impurities.
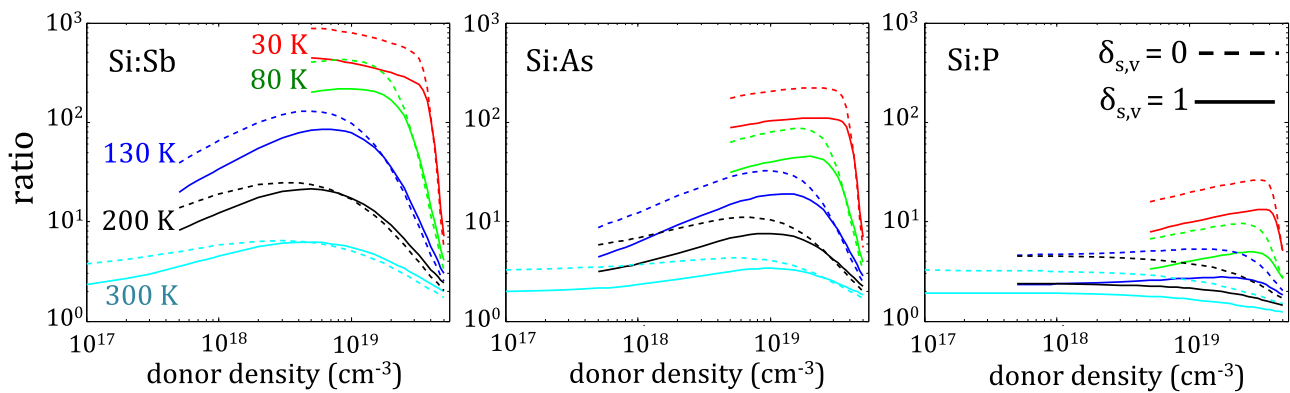

FIG. 5. The relative improvement in the spin relaxation time as a function of donor concentration. The y axis denotes the ratio between the total spin relaxation times for $\Delta_v = 100$ and 0 meV, where Δ_v is the strain-induced valley splitting energy. The solid (dashed) lines show the ratio when the strain and spin orientations are parallel (perpendicular) to each other. At low temperatures (30 and 80 K), the ratio is shown for densities above the metal-to-insulator transition ($N_D > 5 \times 10^{18}$ cm^{-3}), and at intermediate temperatures for densities above $N_D > 5 \times 10^{17}$ cm^{-3} (130 and 200 K). These conditions avoid the freeze-out region in which electrons become localized by the donor potential.
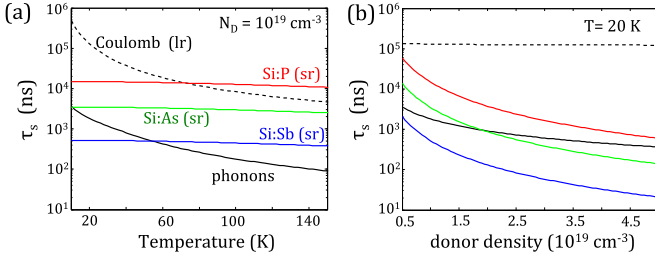
FIG. 6. Spin relaxation times of the various intra-axis mechanisms in strained silicon where $\Delta_v = 120$ meV. Parts (a) and (b) show the dependencies of these mechanisms on temperature when $N_D = 10^{19}$ cm^{-3} and on donor concentration when $T = 20$ K, respectively. Unlike the interaction with the short-range impurity potential, the Coulomb interaction with the long-range ionized impurity potential (dashed lines) and the interaction with phonons (black solid lines) are independent of the donor identity.

The weak dependence of the latter is understood by the fact that the increased donor concentration is accompanied by stronger screening, and the two effects cancel each other (i.e., the relaxation saturates). The enhancement of the intra-axis spin relaxation due to phonons when increasing the donor concentration is understood by the rise of the chemical potential. The phonon wave vector involved in the spin flip of the electron is proportional to $\sqrt{E_F}$ rather than $\sqrt{k_B T}$ in degenerately doped silicon, thereby enhancing the relaxation rate with increasing donor density.

VI. CONCLUSION

We have derived the intra-axis spin-flip matrix elements due to scattering off impurities using Eq. (19), taking into account contributions from both the short-range and long-range parts of the impurity potential. This derivation complements our previous studies of the phonon-induced spin relaxation and the interaxis impurity-induced spin relaxation [18,19,26]. Importantly, the complete analytical framework in Sec. IV allows a fast calculation of the spin relaxation time in n-type silicon due to the interaction of electrons with phonons and impurities for any temperature, strain level, donor identity, and concentration. Depending on the angle between strain and spin orientation, we have provided analytical expressions that quantify the anisotropy in the spin relaxation time.

This work provides a clear motivation for employing silicon spintronic devices in which the spin transport region is compressively strained along one of the crystallographic axes. We have quantified the improvement in the spin relaxation of n-type silicon when applying this type of strain. The spin relaxation time improves evidently when the strain is large enough to depopulate the electrons from the high-energy valleys. In nondegenerate silicon, this condition is met when $\Delta_v \gg k_B T$, where Δ_v is the strain-induced valley splitting energy. In degenerately doped silicon, the condition is met when $\Delta_v - \mu \gg k_B T$, where μ is the chemical potential. The results show that the interaxis elastic impurity scattering is quenched more effectively by the strain compared with the interaxis inelastic phonon scattering. As a result, a larger improvement is expected in degenerately doped Si:Sb compared with Si:P due to the relatively large spin-orbit coupling of Sb, and hence the bigger effect of the electron-impurity interaction

on the spin relaxation in Si:Sb. We have predicted that the spin relaxation time can be enhanced by nearly three orders of magnitude at low-temperature Si:Sb, and by slightly more than one order of magnitude in Si:P under the same strain level, donor concentration, and temperature conditions.

Another finding of our work is that the long-range interaction of electrons with the ionized impurity potential (Coulomb scattering) bears no practical significance for spin relaxation in silicon. It is much weaker than the interaxis spin relaxation mechanisms, and it is also a weak effect when considering the contribution from all other intra-axis mechanisms (especially acoustic phonons or the short-range interaction with impurities in Si:Sb and Si:As). On the other hand, this intra-axis and long-range interaction is known to play a crucial role in limiting the electron mobility of doped semiconductors [26,123–129]. Its insignificance for spin relaxation versus its importance for momentum relaxation implies that estimating the Elliott-Yafet spin relaxation time in n-type silicon by multiplying the momentum relaxation time with some coefficient that depends on the spin-orbit coupling is an arbitrary choice.

APPENDIX A: STRUCTURE OF THE k · p HAMILTONIAN

This appendix includes details on the derivation of the **k · p** Hamiltonian, which we used throughout the main text. Unlike many semiconductors in which the band extrema reside at highly symmetrical points of the Brillouin zone (e.g., the Γ point in GaAs or the L point in germanium), the conduction-band minimum in silicon resides on the Δ-symmetry axis, connecting the Γ and X points. The minimum is located about $0.15(2\pi/a)$ away from the X point ($k_0 = 0.15k_X$). In choosing between the symmetry groups of the Δ axis and the X point to describe the electronic states at the bottom of the conduction bands in silicon, we choose the X point since it has four times more symmetry operations (G_{32}^2 versus C_{4v}). The set of X-point symmetry operations is large enough to determine a compact form of the **k · p** Hamiltonian, and we find that second-order perturbation theory in k_0 produces accurate eigensystem along the Δ axis, despite the fact that k_0 is not negligible.

1. Time-reversal symmetry

We begin with invoking time-reversal argumentation in order to determine whether amplitudes in front of different terms in the Hamiltonian are real or imaginary. The time-reversal operator $\hat{T} = \sigma_y \hat{K}$, where $\hat{K}$ is the operator of complex conjugation, anticommutes with momentum:

$$\hat{\vec{p}} = -i\hbar\nabla \implies \{\mathbf{k} \cdot \mathbf{p}, \hat{T}\} = \mathbf{0}. \tag{A1}$$

TABLE I. Unitary representation of the symmetry operations C_{2y}, S_{4z}, and $\hat{I}$ of the X point along the z axis, $\mathbf{k}_X = (2\pi/a)(1,0,0)$. $\tau = (a/4)(1,1,1)$ denotes the nonprimitive translation, and $\eta = \{E|\mathbf{t}\}$ represents a primitive translation for which $\exp(i\mathbf{k}_X\mathbf{t}) = -1$. See Ref. [115] for more details.

	X_1	X_4
$\{C_{2y}\|0\}$	$-\rho_y$	ρ_y
$\{S_{4z}\|0\}$	$-\rho_y$	$-i\rho_z$
$\{\hat{I}\|\tau\}$	ρ_x	ρ_x
η	$-\rho_0$	$-\rho_0$

From Eq. (2) we conclude that complex conjugation $\hat{K}$ in our basis is represented by ρ_x for both X_1 and X_4. As shown in Table I, the same is true for the inversion $\hat{I}$, so for our basis functions these two operators are identical: $\hat{K} = \hat{I}$. Time-reversal transforms momentum matrix elements as

$$\langle \uparrow X_i|\mathbf{k}\cdot\mathbf{p}|\uparrow X_j\rangle = (\hat{T}\mathbf{k}\cdot\mathbf{p}\uparrow X_j, \hat{T}\uparrow X_i)$$
$$= -\rho_x(\downarrow X_i, \mathbf{k}\cdot\mathbf{p}\downarrow X_j)^*\rho_x$$
$$= \langle \downarrow X_i|\mathbf{k}\cdot\mathbf{p}|\downarrow X_j\rangle^*, \qquad (A2)$$

where the last equality is obtained by applying $\hat{I}$ on top of $\hat{T}$. Analogously,

$$\langle \uparrow X_i|\mathbf{k}\cdot\mathbf{p}|\downarrow X_j\rangle = -\langle \downarrow X_i|\mathbf{k}\cdot\mathbf{p}|\uparrow X_j\rangle^*. \qquad (A3)$$

In a similar fashion, one can transform matrix elements for operators that commute with $\hat{T}$. One of these operators is the spin-orbit interaction of the host crystal (which also commutes with $\hat{I}$),

$$\langle \uparrow X_i|\vec{\nabla}U_{\text{at}}\cdot[\vec{s}\times\hat{\vec{p}}]|\uparrow X_j\rangle$$
$$= -\langle \downarrow X_i|\vec{\nabla}U_{\text{at}}\cdot[\vec{s}\times\hat{\vec{p}}]|\downarrow X_j\rangle^*,$$
$$\langle \uparrow X_i|\vec{\nabla}U_{\text{at}}\cdot[\vec{s}\times\hat{\vec{p}}]|\downarrow X_j\rangle$$
$$= \langle \downarrow X_i|\vec{\nabla}U_{\text{at}}\cdot[\vec{s}\times\hat{\vec{p}}]|\uparrow X_j\rangle^*, \qquad (A4)$$

where U_{at} is the (intrinsic) atomic potential in pure silicon crystal. Finally, we consider operators that represent the impurity potential V and its spin-orbit interaction $\propto\vec{\nabla}V\cdot[\vec{s}\times\hat{\vec{p}}]$. They are not symmetric under inversion, so their time-reversal symmetry relations contain ρ_x matrices:

$$\langle \uparrow X_i|\hat{O}|\uparrow X_j\rangle = \rho_x\langle \downarrow X_i|\hat{O}|\downarrow X_j\rangle^*\rho_x,$$
$$\langle \uparrow X_i|\hat{O}|\downarrow X_j\rangle = -\rho_x\langle \downarrow X_i|\hat{O}|\uparrow X_j\rangle^*\rho_x, \qquad (A5)$$

where $\hat{O} = V$ or $\hat{O} = \vec{\nabla}V\cdot[\vec{s}\times\hat{\vec{p}}]$.

2. Spatial symmetries

The structure of the $\mathbf{k}\cdot\mathbf{p}$ Hamiltonian is determined by matrix elements $\langle X_i|\hat{O}|X_j\rangle$, where $i,j = 1,4$, and $\hat{O}$ can represent $\mathbf{k}\cdot\mathbf{p}$ terms, impurity potential $\hat{V}$, or spin-orbit interaction terms $\vec{\nabla}U_{\text{at}}\cdot[\vec{s}\times\hat{\vec{p}}]$ and $\vec{\nabla}V\cdot[\vec{s}\times\hat{\vec{p}}]$. Let R_i and R_j be IR matrices that represent some symmetry operation $\hat{g}$ acting on X_i and X_j, respectively. The transformation

properties of matrix elements that involve $\hat{O}$ then follow

$$\langle \hat{g}X_i|\hat{g}\hat{O}\hat{g}^{-1}|\hat{g}X_j\rangle = R_i^*\langle X_i|\hat{O}|X_j\rangle R_j^T. \qquad (A6)$$

Following Ref. [115], the operations C_2, S_4, and $\hat{I}$ are sufficient to determine the form of the $\mathbf{k}\cdot\mathbf{p}$ Hamiltonian in the vicinity of the X point. Table I shows the generators of these operations for the chosen conduction (X_1) and valence (X_4) states in Eq. (2).

Below, we demonstrate how the applications of Eq. (A6) and Table I are used to evaluate the nonvanishing interband spin-independent matrix elements of $\hat{O} = \mathbf{k}\cdot\mathbf{p}$. Focusing first on the inversion operation $\hat{I}$ for which $R_1 = R_4 = \rho_x$, we obtain

$$\langle X_1|\mathbf{k}\cdot\mathbf{p}|X_4\rangle = -\rho_x\langle X_1|\mathbf{k}\cdot\mathbf{p}|X_4\rangle\rho_x, \qquad (A7)$$

which means that $\langle X_1|\mathbf{k}\cdot\mathbf{p}|X_4\rangle$ cannot contain any terms proportional to ρ_x or ρ_0. Similarly, we may use other symmetry operations to see further restrictions on $\langle X_1|\mathbf{k}\cdot\mathbf{p}|X_4\rangle$. We see that the terms $k_z(\rho_y,\rho_z)$ are forbidden by S_4^2, and $(k_x\rho_z, k_y\rho_y)$ by C_2. Finally, we are left with the spin-conserving invariant, $H_{cv} \propto ak_x\rho_y + ik_y\rho_z$. By applying S_4 in this expression, we realize that $a = 1$. The spin-independent part of $\langle X_1|\mathbf{k}\cdot\mathbf{p}|X_4\rangle$ is then given by

$$\langle X_1|\mathbf{k}\cdot\mathbf{p}|X_4\rangle = -iP(k_x\rho_y + ik_y\rho_z). \qquad (A8)$$

Thus, using spatial symmetries, we are able to determine that Eq. (A8) represents the spin-independent structure of the off-diagonal (interband) block in our impurity-free Hamiltonian. To see whether the coefficient P in Eq. (A8) is real or imaginary, we will have to employ time-reversal symmetry. For the case of Eq. (A8), Eq. (A2) for $i = 1$ and $j = 4$ makes it clear that the coefficient P in Eq. (A8) is real.

We can apply a similar approach to check which of the spin-dependent terms are symmetry-forbidden. In the absence of impurities, such terms could arise from matrix elements of $\vec{\nabla}U_{\text{at}}\cdot[\vec{s}\times\hat{\vec{p}}]$. We now have to consider not only the orbital parts of R_i and R_j in Eq. (A6), but their spinor-rotation parts as well. In spinor space, the generators of $\hat{I}$, C_2, and S_4 are represented by

$$S(\hat{I}) = -\sigma_0, \quad S(C_2) = i\sigma_y,$$
$$S(S_4) = \frac{\sigma_0 - i\sigma_z}{\sqrt{2}} = \sqrt{-i\sigma_z}, \qquad (A9)$$

where σ_0 is a 2×2 unity matrix acting in spinor space (analogous to $\rho_0 \equiv \mathbb{1}$, which denotes a 2×2 "orbital" unity matrix). Considering first terms that are proportional to ρ_0, we see that $\hat{I}$ allows $(\sigma_0,\sigma_x,\sigma_y,\sigma_z)$, C_2 allows (σ_0,σ_y), and S_4^2 allows (σ_0,σ_z). Thus, $\rho_0\sigma_0$ is the only allowed invariant term. Similarly, we deduce that $\rho_y \otimes \sigma_0$ is forbidden by $\hat{I}$.

3. Intrinsic terms: $\langle X_i|\mathbf{k}\cdot\mathbf{p}|X_j\rangle$ and $\langle X_i|\vec{\nabla}U_{\text{at}}\cdot[\vec{s}\times\hat{\vec{p}}]|X_j\rangle$

The previous section showed how the method of invariants can be used to determine the general form of a $\mathbf{k}\cdot\mathbf{p}$ Hamiltonian [130,131]. Following this method, we have previously derived the spin-dependent Hamiltonian near the X point of

diamond crystal structure [19], finding that

$$H_X = \begin{pmatrix} H_c & H_{cv} \\ H_{cv}^\dagger & H_v \end{pmatrix},$$

$$H_c = \frac{\hbar^2 k_\perp^2}{2m_\perp} + \frac{\hbar^2 k_z'^2}{2m_z} + \hbar v_c k_z' \rho_z,$$

$$H_v = \frac{\hbar^2 k_\perp^2}{2m_\perp} + \frac{\hbar^2 k_z'^2}{2m_z},$$

$$H_{cv} = -iP(k_x \rho_y + ik_y \rho_z) + i\Delta_X(\rho_x \otimes \sigma_y - \rho_0 \otimes \sigma_x)$$
$$+ \alpha k_z'(i\rho_z \otimes \sigma_x + \rho_y \otimes \sigma_y) + \alpha\sigma_z. \quad (A10)$$

Here, $\mathbf{k}' \equiv (\mathbf{k}_\perp, k_z')$, where $k_z' = k_X - k_z$ reaches zero at the X point. The wave-vector component away from the Δ axis, $\mathbf{k}_\perp$, is assumed small enough to be treated perturbatively. While the intraband diagonal blocks, $H_c = \langle X_1 | \mathbf{k} \cdot \mathbf{p} | X_1 \rangle$ and $H_v = \langle X_4 | \mathbf{k} \cdot \mathbf{p} | X_4 \rangle$, are spin-independent (diagonal in spinor space), the interband off-diagonal blocks are affected both by $\mathbf{k} \cdot \mathbf{p}$ and spin-orbit coupling terms. The latter gives rise to two independent crystal parameters, Δ_X and α, as we explain after Eqs. (4) and (6) in the main text. Time-reversal analysis from Appendix A 1 demonstrates that the coefficients v_c, P, Δ_X, and α are real. We emphasize that the resulting form of the Hamiltonian is determined by the representation used in Table I. A different basis choice would result in a different set of generators, and consequently in a different Hamiltonian form.

4. Extrinsic terms: $\langle X_i | \hat{V} | X_j \rangle$ and $\langle X_i | \vec{\nabla} V \cdot [\vec{s} \times \hat{\vec{p}}] | X_j \rangle$

The presence of impurities results in additional perturbative terms. The complete Hamiltonian for a silicon crystal with randomly placed impurities can be written in the mixed momentum-coordinate representation as

$$H(\vec{\rho}, \mathbf{k}) = H_X(\mathbf{k}) + \delta H(\mathbf{k}) \sum_{j=1}^N \chi(\vec{\rho} - \vec{\rho}_j), \quad (A11)$$

where $N = N_D|\Omega|$ is the total number of (randomly placed) defects. $H_X(\mathbf{k})$ is the impurity-free $\mathbf{k} \cdot \mathbf{p}$ Hamiltonian, provided in Eq. (A10), and $\vec{\rho}_j$ denotes the discrete coordinate that lists all of the cells with impurities. The function χ has a value of 1 within unit cells that contain impurities, and 0 otherwise,

$$\chi(\vec{\rho}) = \begin{cases} 1, & \vec{\rho} \in v, \\ 0, & \vec{\rho} \notin v. \end{cases} \quad (A12)$$

To evaluate the form of $\delta H(\mathbf{k})$ in Eq. (A11), we note that the impurity potential, $V(\mathbf{r})$, has two contributions. The first one is invariant with respect to all operations of the diamond point group, while the second contribution transforms according to the IR M_2' of the G_{32}^2 group. The latter flips sign under space inversion operation (it transforms as the product xyz). Repeating the invariant-based analysis in Appendixes A 1 and A 2, we obtain the following impurity-induced interband correction terms (responsible for the Yafet process):

$$\delta H_{cv} = \frac{1}{|v|} \int_v X_1^*(\vec{r})[V(\vec{r}) + \mathbf{k} \cdot \mathbf{p}] X_4(\vec{r}) d^3r$$
$$= -iV_{cv}(\rho_y \otimes \sigma_x + i\rho_z \otimes \sigma_y)$$
$$+ V_{i1} k_z \rho_x \otimes \sigma_0 + V_{i2}(\rho_x k_y - k_x \rho_0) \otimes \sigma_0, \quad (A13)$$

where the X-basis functions are normalized with respect to the elementary cell volume $|v|$,

$$||X_1||_v^2 = ||X_4||_v^2 \equiv \int_v |X_4(\vec{r})|^2 d^3r = |v|. \quad (A14)$$

A different and elegant way to derive the interband invariants in Eq. (A13) is to make use of the selection rules of M_2' with transverse vector components (k_x and k_y) and pseudovector ones (σ_x and σ_y). Transformation properties of the former/latter are represented by M_5/M_5', and their interaction with M_2' flips their roles,

$$M_2' \times M_5 = M_5', \qquad M_2' \times M_5' = M_5. \quad (A15)$$

That is, M_2' switches between the transverse components of vectors (M_5) and pseudovectors (M_5'): $x \leftrightarrow \sigma_x$ and $y \leftrightarrow \sigma_y$. This exchange rule establishes a connection between linear in momentum terms from Eq. (A10) with impurity-induced spin-flip corrections to these equations. For example, let us first inspect the invariant $k_x \rho_y + i k_y \rho_z$ in Eq. (A10), which contains the x and y vector components of $\mathbf{k}$ (M_5 IR). In the disorder-induced part of the Hamiltonian, δH, impurity terms transform according to M_2'. Therefore, we should replace the vector components in $k_x \rho_y + i k_y \rho_z$ with pseudovector ones in order to find the analogous term in δH. The only pseudovector we have is spin, so that δH includes the invariant $\rho_y \otimes \sigma_x + i \rho_z \otimes \sigma_y$ [corresponding to the first term in Eq. (A13)].

To compare the dominant interband spin-mixing terms in Eqs. (A10) and (A13), we make use of the fact that $V_{cv} \sim \delta_B \Delta_{so}$, where $\delta_B = a_B^3/V$, and Δ_{so} is the spin-splitting of the impurity ground state. We get that

	Si : P	Si : As	Si : Sb
$V_{cv}(\text{meV}) \approx$	3.0	10.6	31.3	(A16)

We can now compare the interband spin-mixing amplitude of the impurity with that of the host atoms [V_{cv} in Eq. (A13) versus Δ_X in Eq. (A10)]. The latter gives rise to the interband spin-mixing in clean silicon at $k' = 0$. Given that Si and P are neighboring elements in the Periodic Table, it is reasonable that their spin-orbit coupling parameters are comparable in Si:P, $V_{cv} = 3.0$ meV and $\Delta_X = 3.6$ meV.

Turning to impurity-induced intraband terms, we follow the analysis of Appendix A 2 in order to find the spin-dependent correction of H_c. This correction term is responsible for the central-cell Elliott process,

$$\delta H_c = \delta_B \Delta_0 \rho_0 \otimes \sigma_0 + \delta_B \Delta_1 \rho_y \otimes \sigma_0, \quad (A17)$$

where $\delta_B \Delta_0$ denotes short-range spherically symmetric corrections to the screened Coulomb potential [110]. The second term in Eq. (A17), $\delta_B \Delta_1 \rho_y$, arises due to the low-symmetry (T_d) part of the impurity potential, which is responsible for the spin-independent splitting of the s state into singlet, triplet, and doublet. Finally, the intra-valence-band impurity terms follow,

$$\delta H_v = V_v \rho_z \otimes \sigma_z, \quad (A18)$$

which partially lifts the degeneracy of the valence band near the X point.

APPENDIX B: CORRECTION FACTORS DUE TO THE INTERVALLEY ELECTRON-PHONON INTERACTION

The general expressions for the three intervalley f-process correction factors, $C_{\Sigma_{1-3}}$, that appear in Eq. (22) follow,

$$C_{\Sigma_j} = \frac{3}{\mathcal{I}_1(0) + 2\mathcal{I}_1(\Delta_v)} \frac{1}{A_j r_j K_1(r_j)} \times \{2[e^{-r_j}\mathcal{I}_{+,j}(\Delta_v, \Delta_v - \varepsilon_j) + e^{r_j}\mathcal{I}_{-,j}(\Delta_v + \varepsilon_j, \Delta_v)](1 + B_j\delta_{s,v})$$

$$+ \{e^{-r_j}[\mathcal{I}_{+,j}(\Delta_v, -\varepsilon_j) + \mathcal{I}_{+,j}(0, \Delta_v - \varepsilon_j)] + e^{r_j}[\mathcal{I}_{-,j}(\Delta_v, \varepsilon_j) + \mathcal{I}_{-,j}(\Delta_v + \varepsilon_j, 0)]\}(D_j - R_j\delta_{s,v})\}, \qquad \text{(B1)}$$

where $\{A_j, B_j, D_j, R_j\}$ are, respectively, $\{4, -1, 1, -1\}$ for the Σ_1 mode and $\{8, 1, 3, 1\}$ for the Σ_2 and Σ_3 modes. In addition, $r_j = T_j/2T$ and $\varepsilon_j = k_B T_j$, while $T_1 = 540$ K, $T_2 = 660$ K, and $T_3 = 270$ K. Terms that include e^{r_j} (e^{-r_j}) are associated with phonon emission (absorption). The integral form of $\mathcal{I}_1$ is provided in Eq. (26). The other integral forms are defined as

$$\mathcal{I}_{\pm,j}(\varepsilon_a, \varepsilon_b) = \int_{\varepsilon_m}^{\infty} d\varepsilon \frac{\sqrt{(\varepsilon - \varepsilon_a)(\varepsilon - \varepsilon_b)}}{k_B T} \left[\left.\frac{\partial \mathcal{F}}{\partial \varepsilon}\right|_{\varepsilon} + \mathcal{F}(\varepsilon)\left.\frac{\partial \mathcal{F}}{\partial \varepsilon}\right|_{\pm\varepsilon_j} - \mathcal{F}(\pm\varepsilon_j)\left.\frac{\partial \mathcal{F}}{\partial \varepsilon}\right|_{\varepsilon}\right], \qquad \text{(B2)}$$

where $\varepsilon_m = \max\{\varepsilon_a, \varepsilon_b\}$. The second and third terms in the square brackets stem from the inelastic nature of the scattering ($\varepsilon_j \neq 0$), and they play a role when deviating from the Boltzmann regime. Figures 2(b)–2(d) show the numerical values of $C_{\Sigma_{1-3}}$ as a function of valley splitting energy (Δ_v) for various temperatures and donor concentrations. In the Boltzmann limit, we get

$$C_{\Sigma_j} \to \frac{3e^{-r_v}}{1 + 2e^{-2r_v}} \left\{\frac{2e^{-r_v}}{A_j}(1 + B_j\delta_{s,v}) + \frac{|r_v - r_j|K_1(|r_v - r_j|) + (r_v + r_j)K_1(r_v + r_j)}{A_j r_j K_1(r_j)}(D_j - R_j\delta_{s,v})\right\}, \qquad \text{(B3)}$$

where $r_v = \Delta_v/2k_B T$, and $K_1(x)$ is the first-order modified Bessel function of the second kind.

The general expression for the intervalley g-process correction factor that appears in Eq. (28) follows,

$$C_{\Delta} = \frac{3}{\mathcal{I}_1(0) + 2\mathcal{I}_1(\Delta_v)} \frac{1}{8r_g^2 K_2(r_g)} \times \left\{\left[e^{-r_g}\mathcal{I}_{+,g}(\Delta_v, \Delta_v - \varepsilon_{\Delta_1}) + e^{r_g}\mathcal{I}_{-,g}(\Delta_v, \Delta_v + \varepsilon_{\Delta_1})\right](3 - \delta_{s,v})\right.$$

$$\left. + \left[e^{-r_g}\mathcal{I}_{+,g}(0, -\varepsilon_{\Delta_1}) + e^{r_g}\mathcal{I}_{-,g}(0, \varepsilon_{\Delta_1})\right](1 + \delta_{s,v})\right\}, \qquad \text{(B4)}$$

where $r_g = T_g/2T$ and $\varepsilon_{\Delta_1} = k_B T_g$ ($T_g = 240$ K). In addition,

$$\mathcal{I}_{\pm,g}(\varepsilon_a, \varepsilon_b) = \int_{\varepsilon_m}^{\infty} d\varepsilon \left[\frac{\sqrt{\varepsilon - \varepsilon_a}}{k_B T}\left(\frac{\varepsilon - \varepsilon_b}{k_B T}\right)^{\frac{3}{2}} + \frac{\sqrt{\varepsilon - \varepsilon_b}}{k_B T}\left(\frac{\varepsilon - \varepsilon_a}{k_B T}\right)^{\frac{3}{2}}\right]\left[\left.\frac{\partial \mathcal{F}}{\partial \varepsilon}\right|_{\varepsilon} + \mathcal{F}(\varepsilon)\left.\frac{\partial \mathcal{F}}{\partial \varepsilon}\right|_{\pm\varepsilon_{\Delta_1}} - \mathcal{F}(\pm\varepsilon_{\Delta_1})\left.\frac{\partial \mathcal{F}}{\partial \varepsilon}\right|_{\varepsilon}\right], \qquad \text{(B5)}$$

where $\varepsilon_m = \max\{\varepsilon_a, \varepsilon_b\}$ In the Boltzmann limit, the expression for C_{Δ} becomes compact and is provided by Eq. (34).

---

[1] I. Žutić, J. Fabian, and S. Das Sarma, Rev. Mod. Phys. **76**, 323 (2004).

[2] I. Žutić, J. Fabian, and S. C. Erwin, Phys. Rev. Lett. **97**, 026602 (2006).

[3] H. Dery, Ł. Cywiński, and L. J. Sham, Phys. Rev. B **73**, 161307 (2006).

[4] J. Fabian, A. Matos-Abiague, C. Ertler, P. Stano, and I. Žutić, Acta Phys. Slov. **57**, 565 (2007).

[5] H. Dery, P. Dalal, L. Cywinski, and L. J. Sham, Nature (London) **447**, 573 (2007).

[6] B. Behin-Aein, D. Datta, S. Salahuddin, and S. Datta, Nat. Nanotechnol. **5**, 266 (2010).

[7] Y. Song and H. Dery, Phys. Rev. B **81**, 045321 (2010).

[8] V. Sverdlov and S. Selberherr, Phys. Rep. **585**, 1 (2015).

[9] K. Hamaya, *Spintronics for Next Generation Innovative Devices*, edited by K. Sato and E. Saitoh (Wiley, New York, 2015), Chap. 10.

[10] H. Wen, H. Dery, W. Amamou, T. Zhu, Z. Lin, J. Shi, I. Žutić, I. Krivorotov, L. J. Sham, and R. K. Kawakami, Phys. Rev. Appl. **5**, 044003 (2016).

[11] B. Huang, D. J. Monsma, and I. Appelbaum, Phys. Rev. Lett. **99**, 177209 (2007).

[12] B. Q. Huang, H.-J. Jang, and I. Appelbaum, Appl. Phys. Lett. **93**, 162508 (2008).

[13] J. Li, L. Qing, H. Dery, and I. Appelbaum, Phys. Rev. Lett. **108**, 157201 (2012).

[14] L. Qing, J. Li, I. Appelbaum, and H. Dery, Phys. Rev. B **91**, 241405 (2015).

[15] H. Dery, Y. Song, P. Li, and I. Žutić, Appl. Phys. Lett. **99**, 082502 (2011).

[16] I. Žutić and H. Dery, Nat. Mater. **10**, 647 (2011).

[17] M. I. Dyakonov and V. I. Perel, Sov. Phys. JETP **33**, 1053 (1971) [Sov. Phys. Solid State **13**, 3023 (1972)].

[18] P. Li and H. Dery, Phys. Rev. Lett. **107**, 107203 (2011).

[19] Y. Song and H. Dery, Phys. Rev. B **86**, 085201 (2012).

[20] Y. Yafet, *Solid State Physics*, edited by F. Seitz and D. Turnbull (Academic, New York, 1963), Vol. 14, p. 1.

[21] J. L. Cheng, M. W. Wu, and J. Fabian, Phys. Rev. Lett. **104**, 016601 (2010).

[22] D. Long, Phys. Rev. **120**, 2024 (1960).

[23] H. W. Streitwolf, Phys. Status Solidi B **37**, K47 (1970).

[24] B. K. Ridley, *Quantum Processes in Semiconductors* (Clarendon, Oxford, 1988).

[25] P. Y. Yu and M. Cardona, *Fundamentals of Semiconductors*, 3rd ed. (Springer, Berlin, 2005), Chaps. 2 and 5.

[26] Y. Song, O. Chalaev, and H. Dery, Phys. Rev. Lett. **113**, 167201 (2014).

[27] J.-M. Tang, B. T. Collins, and M. E. Flatte, Phys. Rev. B **85**, 045202 (2012).

[28] P. Li, Y. Song, and H. Dery, Phys. Rev. B **86**, 085202 (2012).

[29] C. Guite and V. Venkataraman, Appl. Phys. Lett. **101**, 252404 (2012).

[30] P. Li, J. Li, L. Qing, H. Dery, and I. Appelbaum, Phys. Rev. Lett. **111**, 257204 (2013).

[31] J. Lohrenz, T. Paschen, and M. Betz, Phys. Rev. B **89**, 121201(R) (2014).

[32] A. Giorgioni, E. Vitiello, E. Grilli, M. Guzzi, and F. Pezzoli, Appl. Phys. Lett. **105**, 152404 (2014).

[33] T. Yu and M. W. Wu, J. Phys.: Condens. Matter **27**, 255001 (2015).

[34] S. Dushenko, M. Koike, Y. Ando, T. Shinjo, M. Myronov, and M. Shiraishi, Phys. Rev. Lett. **114**, 196602 (2015).

[35] J. Ghosh, D. Osintsev, V. Sverdlov, and S. Selberherr, Microelectron. Eng. **147**, 89 (2015).

[36] D. Osintsev, V. Sverdlov, and S. Selberherr, Solid State Electron. **112**, 46 (2015).

[37] Y. Song and S. Das Sarma, Phys. Rev. Appl. **7**, 014003 (2017).

[38] B.-C. Min, K. Motohashi, C. Lodder, and R. Jansen, Nat. Mater. **5**, 817 (2006).

[39] I. Appelbaum, B. Q. Huang, and D. J. Monsma, Nature (London) **447**, 295 (2007).

[40] B. T. Jonker, G. Kioseoglou, A. T. Hanbicki, C. H. Li, and P. E. Thompson, Nat. Phys. **3**, 542 (2007).

[41] M. J. van 't Erve, A. T. Hanbicki, M. Holub, C. H. Li, C. Awo-Affouda, P. E. Thompson, and B. T. Jonker, Appl. Phys. Lett. **91**, 212109 (2007).

[42] H.-J. Jang, J. Xu, J. Li, B. Q. Huang, and I. Appelbaum, Phys. Rev. B **78**, 165329 (2008).

[43] P. Mavropoulos, Phys. Rev. B **78**, 054446 (2008).

[44] S. P. Dash, S. Sharma, R. S. Patel, M. P. de Jong, and R. Jansen, Nature (London) **462**, 491 (2009).

[45] O. M. J. van 't Erve, C. Awo-Affouda, A. T. Hanbicki, C. H. Li, P. E. Thompson, and B. T. Jonker, IEEE Trans. Electron Dev. **56**, 2343 (2009).

[46] H.-J. Jang and I. Appelbaum, Phys. Rev. Lett. **103**, 117202 (2009).

[47] Y. Ando, K. Hamaya, K. Kasahara, Y. Kishi, K. Ueda, K. Sawano, T. Sadoh, and M. Miya, Appl. Phys. Lett. **94**, 182105 (2009).

[48] T. Sasaki, T. Oikawa, T. Suzuki, M. Shiraishi, Y. Suzuki, and K. Tagami, Appl. Phys. Express **2**, 053003 (2009).

[49] C. H. Li, G. Kioseoglou, O. M. J. van 't Erve, P. E. Thompson, and B. T. Jonker, Appl. Phys. Lett. **95**, 172102 (2009).

[50] L. Grenet, M. Jamet, P. Noé, V. Calvo, J.-M. Hartmann, L. E. Nistor, B. Rodmacq, S. Auffret, P. Warin, and Y. Samson, Appl. Phys. Lett. **94**, 032502 (2009).

[51] G. Kioseoglou, A. T. Hanbicki, R. Goswami, O. M. J. van 't Erve, C. H. Li, G. Spanos, P. E. Thompson, and B. T. Jonker, Appl. Phys. Lett. **94**, 122106 (2009).

[52] B. Q. Huang and I. Appelbaum, Phys. Rev. B **82**, 241202(R) (2010).

[53] T. Sasaki, T. Oikawa, T. Suzuki, M. Shiraishi, Y. Suzuki, and K. Noguchi, Appl. Phys. Lett. **96**, 122101 (2010).

[54] T. Sasaki, T. Oikawa, T. Suzuki, M. Shiraishi, Y. Suzuki, and K. Noguchi, IEEE Trans. Mag. **46**, 1436 (2010).

[55] Y. Ando, K. Kasahara, K. Yamane, K. Hamaya, K. Sawano, T. Kimura, and M. Miyao, Appl. Phys. Express **3**, 093001 (2010).

[56] R. Jansen, B. C. Min, S. P. Dash, S. Sharma, G. Kioseoglou, A. T. Hanbicki, O. M. J. van 't Erve, P. E. Thompson, and B. T. Jonker, Phys. Rev. B **82**, 241305(R) (2010).

[57] T. Suzuki, T. Sasaki, T. Oikawa, M. Shiraishi, Y. Suzuki, and K. Noguchi, Appl. Phys. Express **4**, 023003 (2011).

[58] Y. Lu, J. Li, and I. Appelbaum, Phys. Rev. Lett. **106**, 217202 (2011).

[59] Y. Ando, Y. Maeda, K. Kasahara, S. Yamada, K. Masaki, Y. Hoshi, K. Sawano, K. Izunome, A. Sakai, M. Miyao, and K. Hamaya, Appl. Phys. Lett. **99**, 132511 (2011).

[60] J.-C. Le Breton, S. Sharma, H. Saito, S. Yuasa, and R. Jansen, Nature (London) **475**, 82 (2011).

[61] K.-R. Jeon, B.-C. Min, I.-J. Shin, C.-Y. Park, H.-S. Lee, Y.-H. Jo, and S.-C. Shin, Appl. Phys. Lett. **98**, 262102 (2011).

[62] C. H. Li, O. M. J. van 't Erve, and B. T. Jonker, Nat. Commun. **2**, 245 (2011).

[63] T. Sasaki, T. Oikawa, M. Shiraishi, Y. Suzuki, and K. Noguchi, Appl. Phys. Lett. **98**, 012508 (2011).

[64] F. Rortais, C. Vergnaud, C. Ducruet, C. Beigné, A. Marty, J.-P. Attané, J. Widiez, H. Jaffrès, J.-M. George, and M. Jamet, Phys. Rev. B **94**, 174426 (2016).

[65] R. Jansen, Nat. Mater. **11**, 400 (2012).

[66] E. Shikoh, K. Ando, K. Kubo, E. Saitoh, T. Shinjo, and M. Shiraishi, Phys. Rev. Lett. **110**, 127201 (2013).

[67] Y. Pu, P. M. Odenthal, R. Adur, J. Beardsley, A. G. Swartz, D. V. Pelekhov, M. E. Flatté, R. K. Kawakami, J. Pelz, P. C. Hammel, and E. Johnston-Halperin, Phys. Rev. Lett. **115**, 246602 (2015).

[68] J.-H. Lee, S. He, P. Grunberg, M.-J. Jin, J.-W. Yoo, and B. K. Cho, Appl. Phys. Lett. **108**, 032406 (2016).

[69] M. Johnson and R. H. Silsbee, Phys. Rev. B **35**, 4959 (1987).

[70] G. Schmidt, D. Ferrand, L. W. Molenkamp, A. T. Filip, and B. J. van Wees, Phys. Rev. B **62**, R4790 (2000).

[71] E. I. Rashba, Phys. Rev. B **62**, R16267 (2000).

[72] A. Fert and H. Jaffrès, Phys. Rev. B **64**, 184420 (2001).

[73] A. T. Hanbicki, O. M. J. van 't Erve, R. Magno, G. Kioseoglou, C. H. Li, B. T. Jonker, G. Itskos, R. Mallory, M. Yasar, and A. Petrou, Appl. Phys. Lett. **82**, 4092 (2003).

[74] S. A. Crooker, M. Furis, X. Lou, C. Adelmann, D. L. Smith, C. J. Palmstrøm, and P. A. Crowell, Science **309**, 2191 (2005).

[75] M. Shiraishi, Y. Honda, E. Shikoh, Y. Suzuki, T. Shinjo, T. Sasaki, T. Oikawa, K. Noguchi, and T. Suzuki, Phys. Rev. B **83**, 241204(R) (2011).

[76] Y. Ando, K. Kasahara, K. Yamane, Y. Baba, Y. Maeda, Y. Hoshi, K. Sawano, M. Miyao, and K. Hamaya, Appl. Phys. Lett. **99**, 012113 (2011).

[77] L.-T. Chang, W. Han, Y. Zhou, J. Tang, I. A. Fischer, M. Oehme, J. Schulze, R. K. Kawakami, and K. L. Wang, Semicond. Sci. Technol. **28**, 015018 (2013).

[78] O. M. J. van 't Erve, A. L. Friedman, C. H. Li, J. T. Robinson, J. Connell, L. J. Lauhon, and B. T. Jonker, Nat. Commun. **6**, 7541 (2015).

[79] C. Liu, S. J. Patel, T. A. Peterson, C. C. Geppert, K. D. Christie, G. Stecklein, C. J. Palmstrøm, and P. A. Crowell, Nat. Commun. **7**, 10296 (2016).

[80] O. Txoperena and F. Casanova, J. Phys. D **49**, 133001 (2016).

[81] D. J. Monsma, J. C. Lodder, Th. J. A. Popma, and B. Dieny, Phys. Rev. Lett. **74**, 5260 (1995).

[82] R. Jansen, J. Phys. D **36**, R289 (2003).

[83] B. Huang, D. J. Monsma, and I. Appelbaum, J. Appl. Phys. **102**, 013901 (2007).

[84] J. Li, B. Q. Huang, and I. Appelbaum, Appl. Phys. Lett. **92**, 142507 (2008).

[85] J. Li and I. Appelbaum, Appl. Phys. Lett. **95**, 152501 (2009).

[86] Y. Lu, D. Lacour, G. Lengaigne, S. L. Gall, S. Suire, F. Montaigne, and M. Hehn, Appl. Phys. Lett. **103**, 022407 (2013).

[87] D. J. Lépine, Phys. Rev. B **2**, 2429 (1970).

[88] E. M. Gershenzon, N. M. Pevin, and M. S. Fogelson, Phys. Status Solidi B **38**, 865 (1970).

[89] H. Ue and S. Maekawa, Phys. Rev. B **3**, 4232 (1971).

[90] J. D. Quirt and J. R. Marko, Phys. Rev. B **5**, 1716 (1972).

[91] E. M. Gershenzon, N. M. Pevin, and M. S. Fogelson, Phys. Status Solidi B **49**, 287 (1972).

[92] E. M. Gershenzon, N. M. Pevin, and M. S. Fogelson, Phys. Status Solidi B **49**, 411 (1972).

[93] M. Onda and K. Morigaki, J. Phys. Soc. Jpn. **34**, 1107 (1973).

[94] J.-N. Chazalviel, J. Phys. Chem. Solids **36**, 387 (1975).

[95] J. H. Pifer, Phys. Rev. B **12**, 4391 (1975).

[96] Y. Ochiai and E. Matsuura, Phys. Status Solidi A **38**, 243 (1976); **45**, K101 (1978).

[97] V. Zarifis and T. G. Castner, Phys. Rev. B **36**, 6198 (1987).

[98] V. Zarifis and T. G. Castner, Phys. Rev. B **57**, 14600 (1998).

[99] Y. Song and H. Dery, Phys. Rev. Lett. **113**, 047205 (2014).

[100] O. Txoperena, Y. Song, L. Qing, M. Gobbi, L. E. Hueso, H. Dery, and F. Casanova, Phys. Rev. Lett. **113**, 146601 (2014).

[101] G. E. Pikus and A. N. Titkov, in *Optical Orientation*, edited by F. Meier and B. P. Zakharchenya (North-Holland, New York, 1984), Vol. 8, pp. 73–131.

[102] B. D. Gerardot, D. Brunner, P. A. Dalgarno, P. Ohberg, S. Seidl, M. Kroner, K. Karrai, N. G. Stoltz, P. M. Petroff, and R. J. Warburton, Nature (London) **451**, 441 (2008).

[103] C. Lange, G. Isella, D. Chrastina, F. Pezzoli, N. S. Koster, R. Woscholski, and S. Chatterjee, Phys. Rev. B **85**, 241303(R) (2012).

[104] M. Kawano, K. Santo, M. Ikawa, S. Yamada, T. Kanashima, and K. Hamaya, Appl. Phys. Lett. **109**, 022406 (2016).

[105] D. J. Hilton and C. L. Tang, Phys. Rev. Lett. **89**, 146601 (2002).

[106] E. J. Loren, J. Rioux, C. Lange, J. E. Sipe, H. M. van Driel, and A. L. Smirl, Phys. Rev. B **84**, 214307 (2011).

[107] F. Pezzoli, F. Bottegoni, D. Trivedi, F. Ciccacci, A. Giorgioni, P. Li, S. Cecchi, E. Grilli, Y. Song, M. Guzzi, H. Dery, and G. Isella, Phys. Rev. Lett. **108**, 156603 (2012).

[108] A. Baldereschi, Phys. Rev. B **1**, 4673 (1970).

[109] V. F. Gantmakher and Y. B. Levinson, *Carrier Scattering in Metals and Semiconductors (Modern Problems in Condensed Matter Sciences)* (Elsevier, Amsterdam, 1987).

[110] H. I. Ralph, G. Simpson, and R. J. Elliott, Phys. Rev. B **11**, 2948 (1975).

[111] R. L. Aggarwal and A. K. Ramdas, Phys. Rev. **140**, A1246 (1965).

[112] T. G. Castner, Phys. Rev. **155**, 816 (1967).

[113] W. Kohn, in *Solid State Physics*, edited by F. Seitz and D. Turnbull (Academic, New York, 1957), Vol. 5, pp. 257–320.

[114] A. K. Ramdas and S. Rodriguez, Rep. Prog. Phys. **44**, 1297 (1981).

[115] J. C. Hensel, H. Hasegawa, and M. Nakayama, Phys. Rev. **138**, A225 (1965).

[116] H. Jones, *Theory of Brillouin Zones and Electronic States in Crystals* (North-Holland, Amsterdam, 1960).

[117] G. Dresselhaus and M. S. Dresselhaus, Phys. Rev. **160**, 649 (1967).

[118] M. S. Dresselhaus, G. Dresselhaus, and A. Jorio, *Group Theory, Application to the Physics of Condensed Matter* (Springer, Berlin, 2010), Chap. 12.

[119] C. J. Bradley and A. P. Cracknell, *The Mathematical Theory of Symmetry in Solids: Representation Theory for Point Groups and Space Groups* (Clarendon, Oxford, 1972), p. 240.

[120] R. J. Elliott, Phys. Rev. **96**, 266 (1954).

[121] M. Friesen, Phys. Rev. Lett. **94**, 186403 (2005).

[122] T. G. Castner, Phys. Rev. **130**, 58 (1963).

[123] G. Masetti, M. Severi, and S. Solmi, IEEE Trans. Electron Dev. **30**, 764 (1983).

[124] F. J. Morin and J. P. Maita, Phys. Rev. **96**, 28 (1954).

[125] K. B. Wolfstirn, J. Phys. Chem. Solids **16**, 279 (1960).

[126] Y. Furukawa, J. Phys. Soc. Jpn. **16**, 577 (1961).

[127] I. Granacher and W. Czaja, J. Phys. Chem. Solids **28**, 231 (1967).

[128] F. Mousty, P. Ostoja, and L. Passari, J. Appl. Phys. **45**, 4576 (1974).

[129] G. Kaiblinger-Grujin, H. Kosina, and S. Selberherr, J. Appl. Phys. **83**, 3096 (1998).

[130] G. L. Bir and G. E. Pikus, *Symmetry and Strain-Induced Effects in Semiconductors* (Halsted, Jerusalem, 1974), Chaps. 3 and 4.

[131] R. Winkler, *Spin-Orbit Coupling Effects in Two-Dimensional Electron and Hole Systems* (Springer, Berlin, 2003), Appendix B.